UNCLASSIFIED

AD NUMBER

AD871323

NEW LIMITATION CHANGE

TO

Approved for public release, distribution unlimited

FROM

Distribution authorized to U.S. Gov't. agencies and their contractors; Administrative/Operational Use; Feb 1969. Other requests shall be referred to the U.S. Army Missile Command, Attn: AMSMI-RD, Redstone Arsenal, AL. 35809.

AUTHORITY

USAMC ltr, 15 Nov 1972

THIS PAGE IS UNCLASSIFIED

AD871323

AD No. ____
DDC FILE COPY

REPORT NO. RD-TM-69-2

AN EXPERIMENTAL INVESTIGATION OF DOWNSTREAM FLOW-FIELD PROPERTIES BEHIND A SONIC JET INJECTED INTO TRANSONIC FREE STREAM FROM A BODY OF REVOLUTION (SERIES II)

by

C. W. Dahlke

February 1969

This document is subject to special export controls and each transmittal to foreign governments or foreign nationals may be made only with prior approval of this Command, ATTN: AMSMI-RD

U.S. ARMY MISSILE COMMAND
Redstone Arsenal, Alabama. 35809

DDC
JUL 9 1970

FORM AMSMI-1021, 1 DEC 65 PREVIOUS EDITION IS OBSOLETE

20 February 1969 Report No. RD-TM-69-2

AN EXPERIMENTAL INVESTIGATION OF DOWNSTREAM FLOW-FIELD PROPERTIES BEHIND A SONIC JET INJECTED INTO TRANSONIC FREE STREAM FROM A BODY OF REVOLUTION (SERIES II)

by

C. W. Dahlke

DA Project No. 1T061101A91A
AMC Management Structure Code No. 5016.11.8400

This document is subject to special export controls and each transmittal to foreign governments or foreign nationals may be made only with prior approval of this Command, ATTN: AMSMI-RD.

Aerodynamics Branch
Advanced Systems Laboratory
Research and Engineering Directorate (Provisional)
U. S. Army Missile Command
Redstone Arsenal, Alabama 35809

ABSTRACT

Transonic wind-tunnel investigation was conducted to determine the nature of the flow field downstream of a lateral sonic jet on a body of revolution. The survey was made in a plane normal to the body center line 8.63 body diameters aft of the lateral jet nozzle. Velocity measurements were made by a remotely driven pitot-static probe at wind-tunnel Mach numbers of 0.9 and 1.2. The data are presented in the form of Mach number vectors mapped in the normal plane for three pressure ratios and for model angles of attack of 0, 1, and 3 degrees.

Results indicate a pair of trailing vortices in the jet wake on opposite sides of the jet center line. The strength and position appear to be strong functions of pressure ratios and free stream Mach number. These data indicate a method for developing means of determining aerodynamic forces on stabilizing surfaces for missiles with forward jets.

CONTENTS

		Page
1.	Introduction	1
2.	Apparatus	2
3.	Procedures	3
4.	Discussion	3
5.	Conclusions	10
REFERENCES		53
SELECTED BIBLIOGRAPHY		54

ILLUSTRATIONS

Figure		Page
1	Flow Angle Probe	12
2	Model and Probe with Survey Grid Installed in 8-Foot Test Section	13
3	Model and Probe with Survey Grid Installed in 8-Foot Test Section	14
4	Mach Number Vector Coordinate Geometry	15
5	Model and Survey Grid Geometry	16
6	Jet Wake in Free Stream Flow Field at Mach 0.9 and Zero Angle of Attack	17
7	Jet Wake in Free Stream Flow Field at Mach 0.9 and Zero Angle of Attack	18
8	Jet Wake in Free Stream Flow Field at Mach 0.9 and Zero Angle of Attack	19
9	Jet Wake in Free Stream Flow Field at Mach 0.9 and Zero Angle of Attack	20
10	Jet Wake in Free Stream Flow Field at Mach 0.9 and Zero Angle of Attack	21
11	Jet Wake in Free Stream Flow Field at Mach 1.2 and Zero Angle of Attack	22
12	Jet Wake in Free Stream Flow Field at Mach 1.2 and Zero Angle of Attack	23
13	Jet Wake in Free Stream Flow Field at Mach 1.2 and Zero Angle of Attack	24
14	Jet Wake in Free Stream Flow Field at Mach 1.2 and Zero Angle of Attack	25

ILLUSTRATIONS (Concluded)

Figure		Page
15	Jet Wake in Free Stream Flow Field at Mach 1.2 and Zero Angle of Attack	26
16	Lower Vortex Core Coordinates	27
17	Vortex Pattern	28
18	Vortex Strengths	29
19	Computed Flow Field for Mach 0.9 and α = 0 Degree	30
20	Computed Flow Field for Mach 0.9 and α = 0 Degree	31
21	Computed Flow Field for Mach 0.9 and α = 0 Degree	32
22	Computed Flow Field for Mach 0.9 and α = 0 Degree	33
23	Computed Flow Field for Mach 1.2 and α = 0 Degree	34
24	Computed Flow Field for Mach 1.2 and α = 0 Degree	35
25	Computed Flow Field for Mach 1.2 and α = 0 Degree	36
26	Computed Flow Field for Mach 1.2 and α = 0 Degree	37
27	Computed Flow Field for Mach 1.2 and α = 0 Degree	38
28	Flow-Field Theory Upwash Comparisons	39
29	Flow-Field Theory Upwash Comparisons	40
30	Free Stream Flow Field	41
31	Free Stream Flow Field	42
32	Perturbation of Free Stream Flow Field	43
33	Perturbation of Free Stream Flow Field Due to Jet Wake and Angle of Attack	44
34	Perturbation of Free Stream Flow Field Due to Jet Wake and Angle of Attack	45
35	Perturbation of Free Stream Flow Field Due to Jet Wake and Angle of Attack	46
36	Perturbation of Free Stream Flow Field Due to Jet Wake and Angle of Attack	47
37	Perturbation of Free Stream Flow Field Due to Jet Wake and Angle of Attack	48
38	Perturbation of Free Stream Flow Field Due to Jet Wake and Angle of Attack	49
39	Free Stream Flow Field Due to Jet Wake and Angle of Attack	50
40	Perturbation of Free Stream Flow Field Due to Jet Wake and Angle of Attack	51
41	Free Stream Flow Field Due to Jet Wake and Angle of Attack	52

SYMBOLS

a	Speed of sound (~ ft/sec)
D	Model diameter (5.5 in.)
d_j	Jet exit diameter
f	Vortex center outboard coordinate (in.)
h	Vortex center vertical coordinate (in.)
ℓ	Distance from jet center line to probe station
M	Mach number
M_X, M_Y, M_Z	Components of Mach Number along X, Y, Z coordinates, respectively
P	Pressure
P_1-P_6	Probe pressures
R	Body radius (2.75 in.)
V	Velocity
X, Y, Z	Rectangular coordinates, X, along model center line with origin at nose apex
α	Angle of attack, pitch plane (deg)
Γ	Vorticity or vortex strength (~ ft^2/sec)
ψ	Angle of attack, yaw plane (deg)

Subscripts

c	Plenum chamber
i	Image vortex
j	Jet conditions
ℓ	Vortex (lower) below jet center line
p	Probe measured parameter
u	Vortex (upper) above jet center line
∞	Free stream condition

ACCESSION for
CFSTI WHITE SECTION ☐
DDC BUFF SECTION ☐
UNANNOUNCED ☐
JUSTIFICATION .....
.....
BY.....
DISTRIBUTION/AVAILABILITY CODES
DIST. AVAIL. and/or SPECIAL
2

DISPOSITION INSTRUCTIONS

Destroy this report when it is no longer needed. Do not return it to the originator.

DISCLAIMER

The findings in this report are not to be construed as an official Department of the Army position unless so designated by other authorized documents.

1. Introduction

Currently, the missile aerodynamicist is confronted more and more with the problem of assessing the flow interaction interference produced by injecting a secondary gas stream into the primary flow field. Such cases occur when reaction jets are used for control, to provide a spin impulse, or where residual gases from pressurization systems and similar devices are expelled. When these gases are injected near the nose of the missile body, it has been observed that large changes occur in the stability, control, and rolling moment characteristics. This effect has been attributed largely to the resulting changes in the flow field over the fin stabilizing surfaces.

Previous analytical and experimental research studies have concentrated on the flow-field interaction in the vicinity of the secondary jet exit. Most of the studies have considered the two-dimensional problem with a supersonic primary flow. Little has been accomplished in determining the flow-field properties induced by the jet at large distances downstream of the injection point.

The present study is the second series of wind-tunnel tests that attempt to provide some insight into the details of the perturbed flow field which was observed to produce large changes in the aerodynamic loads of missile stabilizing surfaces.

The detailed flow-field structure was measured by a six-tube yaw head pressure probe which was calibrated to give the local Mach number, dynamic pressure, and the pitch and yaw angles of the local velocity vector. The basic model configuration was a body of revolution with a four-caliber ogive nose and a cylindrical afterbody. A single circular sonic nozzle was located three body diameters from the body apex with its axis normal to the body center line and oriented radially in the yaw plane. The flow field was surveyed in a plane normal to the body center line 8.63 body diameters aft of the lateral jet nozzle. Measurements were made in the Cornell Aeronautical Laboratory (CAL) 8-foot transonic wind tunnel at free stream Mach numbers 0.9 and 1.2, angles of attack of 0, 1, and 3 degrees, and jet-chamber-to-free-stream static pressure ratios of 0, 10, 20, 30, 40, and 80.

The basic results are presented in the form of graphs mapping the Mach number in a plane normal to the body's longitudinal axis. The qualitative effects of free stream Mach number, jet-pressure ratio, and angle of attack are illustrated in these plots.

2. Apparatus

The test was conducted in CAL's 8-foot transonic wind tunnel. The test setup consisted of a model (body of revolution) mounted on a sting, and a movable pitot-static probe was mounted on the tunnel strut such that flow-field points around the vicinity of the aft end of the model could be measured.

The model had a four-caliber tangent ogive nose with a 9.89-caliber afterbody. The cylinder diameter was 5.5 inches. A lateral jet was located three calibers from the nose apex. The nozzle was circular with a sonic exit 0.44 inch in diameter. Model attitude was maintained by a bubble for all angles of attack. The model was suspended from the sting by a five-component strain gage balance which had been previously designed and built by CAL for the U. S. Army Missile Command (MICOM), Redstone Arsenal, Alabama. The balance measurements were not required for this test; however, they were recorded. A total pressure orifice and a thermocouple were installed in the jet plenum chamber.

The flow-angle probe was supplied by CAL (Figure 1). This probe has a hemispherical head 3/16 inch in diameter. The hemisphere has pressure orifices located at the center and 45 degrees each side of the center in both pitch and yaw planes. A ring of static pressure orifices connected to a common manifold on the cylindrical part of the probe was located 10 diameters behind the head. All pressures were routed to a scanivalve on the probe support.

Figures 2 and 3 show the model and probe installed together in the 8-foot test section with the survey grid attached to model. The grid was used to predetermine the stops for the probe during the test and to spot-check settings at selected times during the test. The grid was removed during the actual test.

The probe forward end was 11.58 body diameters aft of the nose apex. The lateral probe position was achieved by rotation within the probe mount, and the vertical position by translation of the model and sting on the tunnel strut. A smaller roll mechanism was used to level the forward probe orifices at each of the lateral probe positions.

The goemetric angles were estimated by CAL to be accurate to ±0.02 degree. The probe local flow angles, as deduced from the probe calibrations, are accurate to ±0.2 degree within the linear range of ±6 degrees. The transducer measuring plenum chamber pressure was calibrated to an accuracy of ±1.0 psi.

3. Procedures

The test was conducted at tunnel free stream Mach Numbers of 0.9 and 1.2. These were the two Mach numbers for which CAL had calibrated the flow-angle probe. Flow-field surveys at these two Mach numbers were conducted at model plenum chamber pressure to tunnel free stream static pressure ratios of 0 (jet off) 10, 20, 40, and 80. The probe was always aligned parallel to the tunnel center line. The survey was conducted over a plane always normal to the model center line. This plane is defined by rectangular coordinates Y, Z with the origin being on the model center line at 11.58 model diameters (calibers) from the nose apex. The lateral coordinate Y was obtained by a remote roll mechanism allowing the probe to be moved away from the model in an arc, and the vertical coordinate Z was obtained by vertical translation of the model and sting on the tunnel strut. This way displacement was achieved both horizontally and vertically. One run usually consisted of fixing Mach number, model angle of attack, P_c/P_∞, and the lateral position Y while the model was translated vertically with predetermined stops Z to take data (normally 1.0-in. increments). A complete run consisted of measurements at all grid points for fixed pressure ratio, Mach number, and angle of attack. Local Mach number was computed by:

$$M_p = \left[5\left(\frac{P_5}{P_6}\right)^{2/7} - 5 \right]^{1/2} ,$$

where P_5 was the measured stagnation pressure (center orifice), and P_6 was measured static pressure. Angles in the pitch α_p and yaw ψ_p direction were determined by comparing differential pressures on the orifices 45 degrees around spherical nose $P_2 - P_1$ (pitch) and $P_3 - P_4$ (yaw) to the previously calibrated differential pressure as a function of pitch and yaw angles. The data output consisted of tunnel conditions, model plenum chamber (nitrogen) condition, geometric setup (i.e., α, Y, Z), and the probe outputs.

4. Discussion

The data reduction by CAL included a computation of the local Mach number M_p measured by the probe and angles in pitch α_p and yaw ψ_p determined from probe differential pressure measurement [1] and previous calibrations. The survey coordinates were taken in the rectangular coordinate system with the origin being the model center line at X = 11.58 calibers from the nose apex. Figure 4 shows a goemetric representation of the flow angularity in the

X, Y, Z coordinate system, the longitudinal X, lateral Y, and vertical Z. Mach number components are computed with the following relations, respectively:

$$M_X = M_p \cos \phi_p \cos \alpha_p$$

$$M_Y = M_p \sin \phi_p \cos \alpha_p$$

$$M_Z = M_p \cos \phi_p \sin \alpha_p \quad .$$

The pitch angle α_p used in these equations consists of the probe measured pitch angle plus the model goemetric angle of attack. The sign convention specifies that from an aft view, positive vectors are to the right and up along Y-Z, respectively.

From the onset the object of these flow-field surveys has been an attempt to explore the downstream phenomena that cause a jet gas and free stream interaction to induce forces on missile stabilizing surfaces. The first flow-field survey (April 1967) conducted during this study was based on an arbitrary selection of survey grid points [2]. A useful result of the April 1967 test was that future tests could be planned more efficiently. This was the major factor in selection of grid points for this survey. The grid limits and spacing of points were selected to contain the trailing vortices indicated from the 1967 results. Part of this survey fills in gaps of the first survey, but most of the time was spent in an attempt to achieve enough points to define the location and vorticity of the vortex cores. Particular emphasis was made at zero angle of attack, where it is felt the basic phenomena must be understood. To fulfill the requirements for the survey zone the probe mount was modified by CAL to give lateral movement from the model center line Y = 0 to Y = -15 inches, with a vertical travel of Z = ±6 inches (Figure 5). This allows points to be surveyed beyond the core for the most outboard core position investigated. Because of the new mount and model installation differences, the probe was 2.59 inches (0.47 cal.) further forward for this test than the April 1967 entry. The rest of the geometry was identical to the april 1967 entry with the jet again in the lateral plane (Figure 5).

a. Zero Angle of Attack Case

It was felt in the beginning of this study that if one could understand the flow-field mechanics of the jet wake downstream this would be a gigantic building stone toward piecing together the complete story of the jet free stream interaction and its effect on missile stabilizing surfaces; however,

there are many parameters involved. Because of the limited time that is available for testing, some of these parameters were fixed while others thought to be more important or more readily available were investigated. The model geometry and the nozzle were two important parameters that were fixed. The nozzle was sonic with a 0.44-inch throat (exit diameter), and this was thought to be a case which could be a base for later nozzle parametric studies. It seems that the trends with other parameters such as angle of attack, Mach number, and jet chamber to free stream pressure ratio would be the same with superonsic nozzles, even though the magnitudes of the flow-field parameters may be different. Three important parameters, Mach number, angle of attack, and pressure ratio, were varied over limited ranges. Mach numbers were restricted to the two for which the probe was calibrated in the CAL 8-foot wind tunnel. The pressure ratio of jet chamber to free stream static was varied over a range that appears in practical application to Army systems. This section will present the survey results for the case of zero angle of attack. The data are presented in the form of velocity vectors in the Y-Z plane originating from their respective coordinates on a scaled grid.

These velocity vectors are:

$$|M_{YZ}| = \sqrt{M_Y^2 + M_Z^2}$$

$$\tan^{-1} \phi = M_Y/M_Z$$

where M_Y, M_Z, and ϕ are defined in Figure 4.

Figures 6 through 15 show these vector diagrams of the cross flow pattern for Mach numbers 0.9 and 1.2 at all pressure ratios P_c/P_∞ tested. Figures 6 through 10 show the flow-field pattern at $M_\infty = 0.9$ for $\alpha = 0$ degree. The survey limits vary for each P_c/P_∞ because of the dependence of the vortex core position on pressure ratio. These limits were chosen from the estimated core position from the earlier test. The probe travel had the limitation of $Y \leq 8.5$ inches during the earlier test; therefore, the core position had not been defined. However, estimates were made based on the data that were available. These estimates [2] were then used to determine the grid size for each M_∞ and P_c/P_∞. It has been assumed that because of geometric symmetry at $\alpha = 0$ degrees, symmetry would exist in the flow field where geometric symmetry exists. These data were corrected for small flow angularity that was observed for the jet-off case, forcing the vectors along $Z = 0$ to have small M_Z components as would be expected with symmetry.

The test plan was made to take advantage of the symmetry by planning to survey only one side of the line of symmetry. For $P_c/P_\infty = 40$ this assumption was checked (Figure 8) by making the survey on both sides of the line $Z = 0$. It can be seen from Figure 8 that there is a symmetrical pair of vortices about the line $Z = 0$, at least within the accuracy of the data. The data during the initial run at $P_c/P_\infty = 20$ at the even inch coordinates are questionable, and intermediate points were picked up later during the test. The points at the even coordinates were omitted for $Z < 2$ at $P_c/P_\infty = 20$. The lower half of $P_c/P_\infty = 40$ was plotted on a larger scale (Figure 9) to aid in determinating the vortex coordinates, f, h, and the vorticity Γ/a. The scales for the magnitude of $\overline{M_{YZ}}$ are noted on each plot. From these plots at $M_\infty = 0.9$ a set of lower vortex coordinates f_ℓ and h_ℓ were chosen, with the upper vortex coordinates assumed to be $f_u = f_\ell$ and $h_u = -h_\ell$. These coordinates are plotted versus P_c/P_∞ in Figure 16, where the coordinates f_ℓ, f_u, h_ℓ, and h_u are defined in Figure 17 as being lateral and vertical referenced to the model center line. At $P_c/\Gamma_\infty = 20$ and 80 (Figures 7 and 10) the vectors shown by dashed lines are the April 1967 data plotted for comparison. The data match as well as can be expected considering the basic accuracy of the test setup and that the data are from different entries.

Figures 11 through 15 show the Mach number 1.2 data at zero angle of attack and $P_c/P_\infty = 10$, 20, 30, 40, and 80. The only basic differences between these data and the Mach 0.9 are the position above and below the line of symmetry of the core center and the magnitude of the vector $\overline{M_{YZ}}$ or vorticity. Comparison of the plots of $M_\infty = 0.9$ and the Mach 1.2 vectors shows the higher Mach number compresses the vortex pair closer together. The coordinates of the lower vortex as determined from these plots are shown in Figure 16. The $P_c/P_\infty = 20$ case was surveyed on both sides of the line $Z = 0$ (Figure 12). The dashed vectors on Figures 12 and 15 are the data at $P_c/P_\infty = 20$ and 80, respectively, from the first survey of April 1967 [2]. There is good agreement at $P_c/P_\infty = 80$; however, there appears to be a loss in quality of data from this test at $P_c/P_\infty = 20$.

b. Vorticity

The position of the vortex centers at both Mach 0.9 and 1.2 was obtained from the plots of $\overline{M_{YZ}}$, and these coordinates were used in a computer program to re-compute the M_{YZ} vectors for the quantity $\Gamma/a = 1$. The ratio of vorticity Γ to local speed of sound a was used because Mach number vectors were plotted rather than velocity.

The equations used for computing the Mach number vectors are

$$M_Y = \frac{V_Y}{a} = -\frac{\Gamma}{a}\frac{1}{2\pi}\left[\frac{Z - h_\ell}{\left(Y - f_\ell\right)^2 + \left(Z - h_\ell\right)^2} - \frac{Z - h_{\ell i}}{\left(Y - f_{\ell i}\right)^2 + \left(Z - h_{\ell i}\right)^2}\right.$$

$$\left. - \frac{Z - h_u}{\left(Y - f_u\right)^2 + \left(Z - h_u\right)^2} + \frac{Z - h_{ui}}{\left(Y - f_{ui}\right)^2 + \left(Z - h_{ui}\right)^2}\right]$$

$$M_Z = \frac{V_Z}{a} = \frac{\Gamma}{a}\frac{1}{2\pi}\left[\frac{Y - f_\ell}{\left(Y - f_\ell\right)^2 + \left(Z - h_\ell\right)^2} - \frac{Y - f_{\ell i}}{\left(Y - f_{\ell i}\right)^2 + \left(Z - h_{\ell i}\right)^2}\right.$$

$$\left. - \frac{Y - f_u}{\left(Y - f_u\right)^2 + \left(Z - h_u\right)^2} + \frac{Y - f_{ui}}{\left(Y - f_{ui}\right)^2 + \left(Z - h_{ui}\right)^2}\right],$$

where

$$f_i = \frac{fR^2}{f^2 + h^2}$$

and

$$h_i = \frac{hR^2}{f^2 + h^2}$$

R = body cylindrical radius.

The plots of these for Γ/a unity were then compared to the test data by overlays. The vector directions were compared for all coordinates except those near the vortex core. Small changes in the first estimates of the core positions were made to make the best match of vector direction. Then the vector length ratio of the test to computed data was averaged for several vectors located sufficiently far from the vortex core viscous region. The

equations here are from plane vortex theory and are invalid where the velocity gradients become large and viscosity is dominant. These equations have large gradients near the core approaching a singular point at the core center. At positions sufficiently far from the center of the vortex the velocity gradients are small enough to cause the plane vortex theory to be useful in matching these test data. The ratio of $|M_{YZ}|$ from test to $|M_{YZ}|$ for a $\Gamma/a = 1$ was used to modify Γ/a so that the magnitude as well as direction agrees fair throughout the region of the test. The values of Γ/a are presented versus P_c/P_∞ in Figure 18, and plots of $\overline{M_{YZ}}$ at their respective coordinates are shown in Figures 19 through 27. Because of the viscosity near the core region the velocity gradient is not as steep as the theory predicts, and the plane vortex theory will not match vectors in this region.

c. Angle-of-Attack Case

It is important to know what the flow-field mechanics are for the basic case of zero angle of attack; however, from a practical viewpoint the ultimate goal for a study of jet free stream interaction is to formulate models, both physical and mathematical, that can be useful for definition of the forces on the downstream stabilizing surfaces. Due to the exploratory nature of this experiment a sample of cases was tested with a geometric angle between the model and the wind-tunnel free stream flow. The time available for this test together with the time required to make measurements limited the amount of angle of attack data that was obtained. Out of these tests it was desired to determine if the nature of the flow significantly changes from the zero alpha case. Two angles of attack were investigated during this study. It has been shown [3-6] that the most significant change in stabilizing surface forces occurs at small angles of attack. Based on this, angles of attack of 1 and 3 degrees were chosen for this test. One run was made for $\alpha = -3$ degrees, but this was for testing convenience, and because of symmetry should yield results that are negative of the run at $\alpha = 3$ degrees.

One case of angle of attack without the jet was run during the April 1967 test [2]. This was at Mach number of 0.9 and alpha of 1 degree. The cross flow vectors $\overline{M_{YZ}}$ were plotted at their respective coordinates, and the row at $Z = 0$ was compared to Beskin's upwash theory. A survey was made during this test for two additional angles of attack, 3 degrees at $M_\infty = 0.9$ and 1 degree at $M_\infty = 1.2$. Figures 28 and 29 show the comparison of the row of vectors at $Z = 0$ to Beskin's upwash theory [6] for each of these cases respectively. Figures 30 and 31 show the vectors $\overline{M_{YZ}}$ plotted for all survey

grid points for these two jet-off cases. For these two plots the angle of attack is included in the vector component M_Z, where Figure 32 shows the cross flow vector $\overline{M_{YZ}}$ without the angle of attack of 3 degrees, or this shows the perturbation velocity induced by angle of attack. The vectors on Figure 32 are derived from direct measurement, since the probe was always at zero angle of attack relative to the wind-tunnel test section velocity vector, where the velocity vectors shown in Figures 30 and 31 have the geometric pitch angle of attack added to the probe measured angle in the pitch plane. The perturbation velocities are not shown for $M_\infty = 1.2$ and $\alpha = 1$ degree because their inherent small magnitude coupled with the probe accuracy makes this type of presentation rather meaningless. These data without the jet show the overall accuracy of the probe measurement system to be adequate for detailed studies of flow fields of this type.

Several runs were made at angle of attack with the jet pressure on (Figure 5) at Mach numbers 0.9 and 1.2. The procedure for setting the Y-Z probe coordinates was modified during the angle of attack runs. At each angle of attack change the probe setting on the Z-axis had to be changed. The scheme was to indicate a touch through an electrical ground system and then to re-zero the vertical translation of the model strut assembly. In several runs the tunnel operators failed to do this and the survey field was in the wrong zone to pick up the primary effects of the downstream jet at angle of attack. The results at angle of attack with the jet on are in general not up to par with the zero angle of attack data in quality. There are several runs, however, that show distinct patterns of the twin vortex combined with the body cross flow, and these are believed to be typical. Those cases where the vortex flow is apparent show that the position of the vortices at a downstream position tend to be slightly above the trailing streamline emanating from the jet exit. This is expected since the upwash flow around the body at angle of attack increases the local angle of attack in the vicinity of the body. Figures 33 and 34 show the velocity vectors $\overline{M_{YZ}}$ induced by jet and body upwash at their respective coordinates for $P_c/P_\infty = 20$ at $\alpha = 1$ and 3 degrees, respectively, with a free stream Mach number of 0.9. The $\alpha = 1$ degree case (Figure 33) is somewhat as expected; however, the 3-degree case (Figure 34) does not have a clear definitive flow pattern. The only explanation of this plot is that there was a loss in quality of data during part of this configuration due to some unknown cause. Figure 35 shows the circulation clearly, and shows how the shift occurs from the zero angle of attack case. This case is for $P_c/P_\infty = 40$ and $\alpha = 1$ degree. Because of the higher pressure ratio the vorticity is stronger (Figure 18) than for $P_c/P_\infty = 20$ (Figures 33 and 34), and this accounts for some of the better defined flow, which brings up a question that these data do not fully answer. Does the angle

of attack cause a loss in identity of the vortex pattern at these pressure ratios and distances downstream? If it does then the next problem is to determine at what combination of angle of attack, pressure ratio, and distance downstream that this occurs. There is, in all cases from these data, a better defined flow field for the higher pressure ratios. This can be observed in Figures 38 through 41 for Mach number 1.2 case where higher pressure ratios show the more complete vortex pattern and the associated shift with angle of attack. Figures 36 and 37 again show $P_c/P_\infty = 20.0$ at $\alpha = 1$ and 3 degrees, respectively, for Mach number of 1.2. These plots do not have the angle of attack added, and represent only the jet and body upwash induced velocities. These are somewhat better than the M = 0.9 data for the same configuration, but are not as clear as the equivalent plots for M = 1.2, $P_c/P_\infty = 40.0$, and 80.0 at $\alpha = 1$ degree (Figures 38 and 40). Figures 39 and 41 show the angle of attack component of 1 degree added to the probe measured component for the computation of the vector $\overline{M_{YZ}}$. Shown on all plots at angle of attack are the locations of the estimated vortex core for corresponding zero angle of attack cases. This shows directly the shift that occurs in the mixed flow field due to angle of attack.

5. Conclusions

A wind-tunnel flow-field survey of the downstream wake from a lateral jet located on the forward portion of a body of revolution was conducted at transonic Mach numbers of 0.9 and 1.2. The test was conducted for several jet chambers to free stream pressure ratios and angles of attack. This series of tests has lead to the following conclusions:

a) This unique means of using a six-hole pitot-static probe to survey the downstream jet wake in the presence of a body of revolution has proven to be an adequate method of defining the flow-field mechanics.

b) The flow-field model established from results of this test consists of a pair of trailing vortices on opposite sides of the jet center line, with the vortex centers and vorticity appearing to be primarily function of jet chamber pressure to free stream static pressure ratio and free stream Mach number.

c) The angle of attack case shows a shift in the vortex core location that is located in the vicinity of a streamline emanating from the jet center line and trailing aft in the direction of free stream flow. The flow angularity induced by the body at angle of attack causes some further shift in the vortex core position.

d) The flow field at zero angle of attack can be matched reasonably well with plane vortex theory using the vortex core location and strength as the foundation.

e) Future test planning can be augmented through use of these results for a more powerful study.

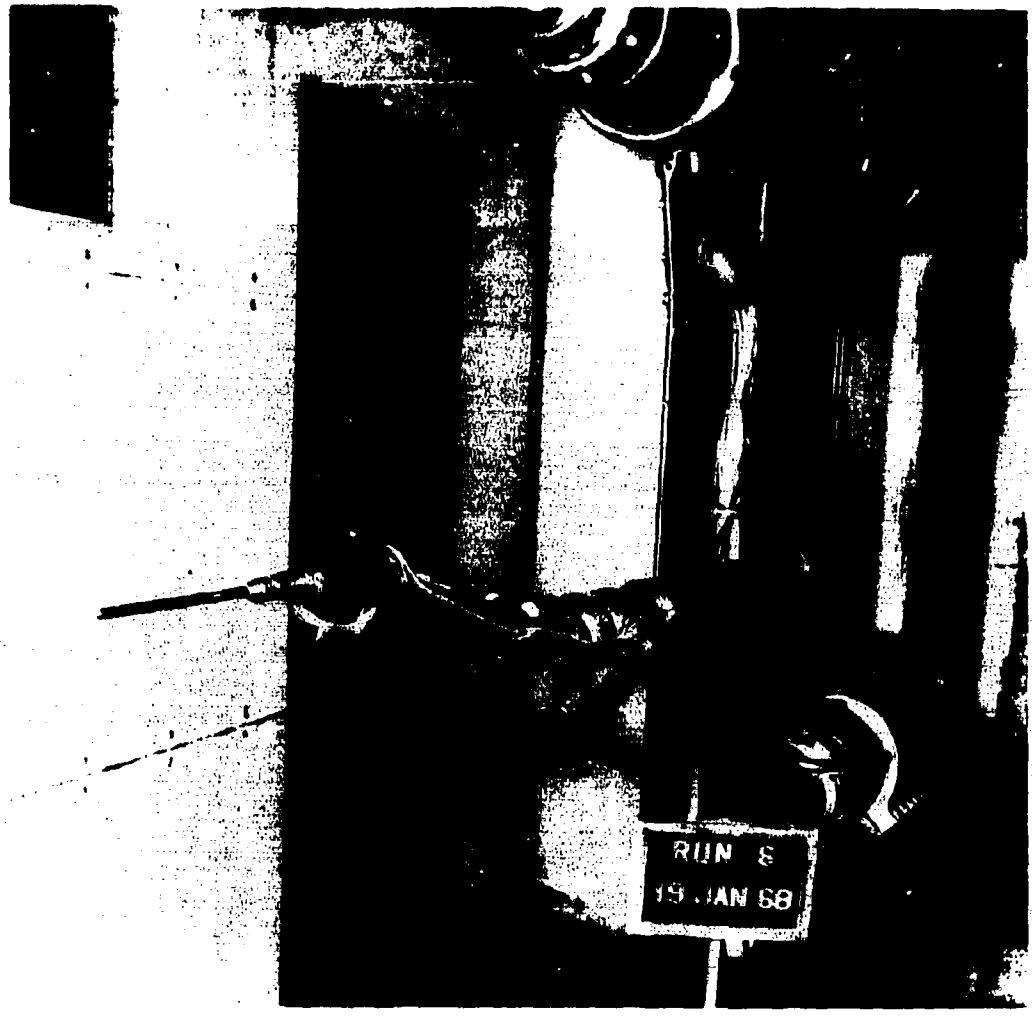

FIGURE 1. FLOW ANGLE PROBE

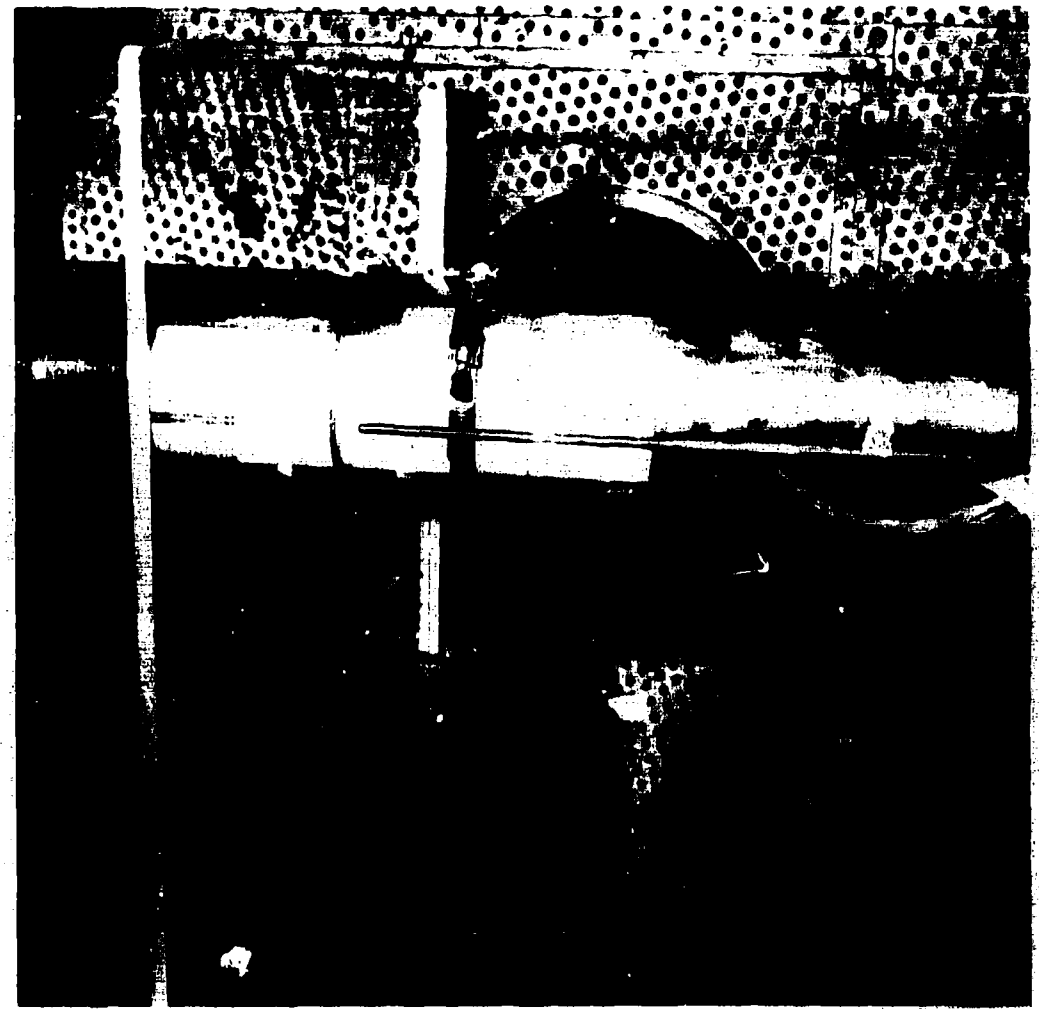

FIGURE 2. MODEL AND PROBE WITH SURVEY GRID INSTALLED IN 8-FOOT TEST SECTION

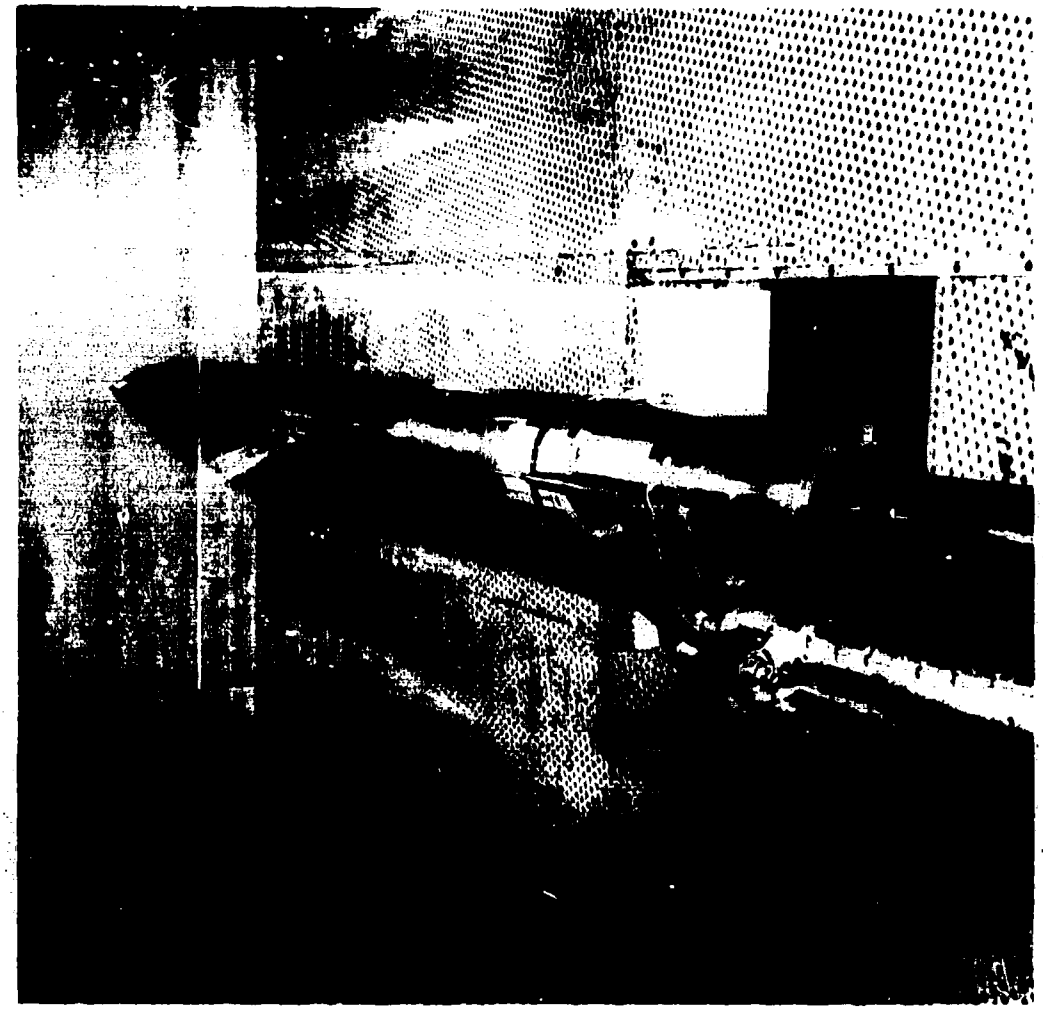

FIGURE 3. MODEL AND PROBE WITH SURVEY GRID INSTALLED IN 8-FOOT TEST SECTION

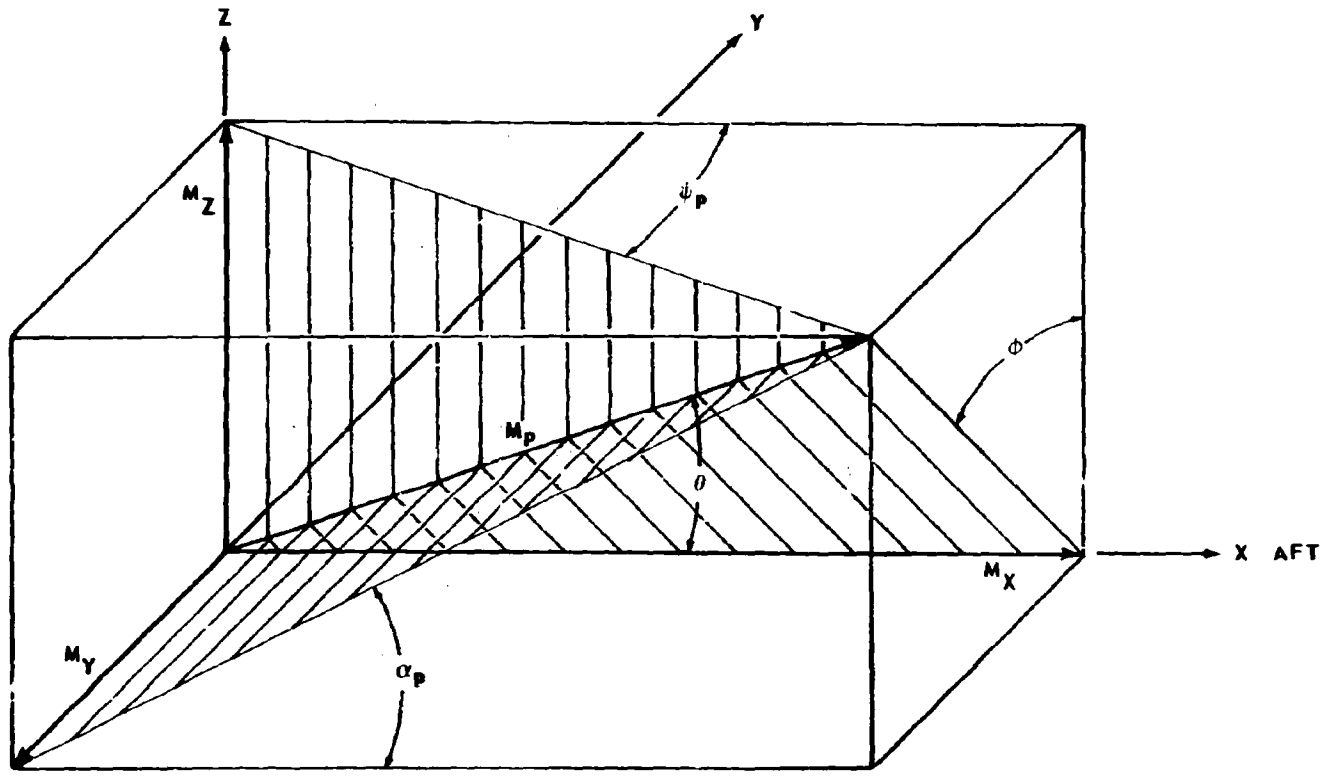

FIGURE 4. MACH NUMBER VECTOR COORDINATE GEOMETRY

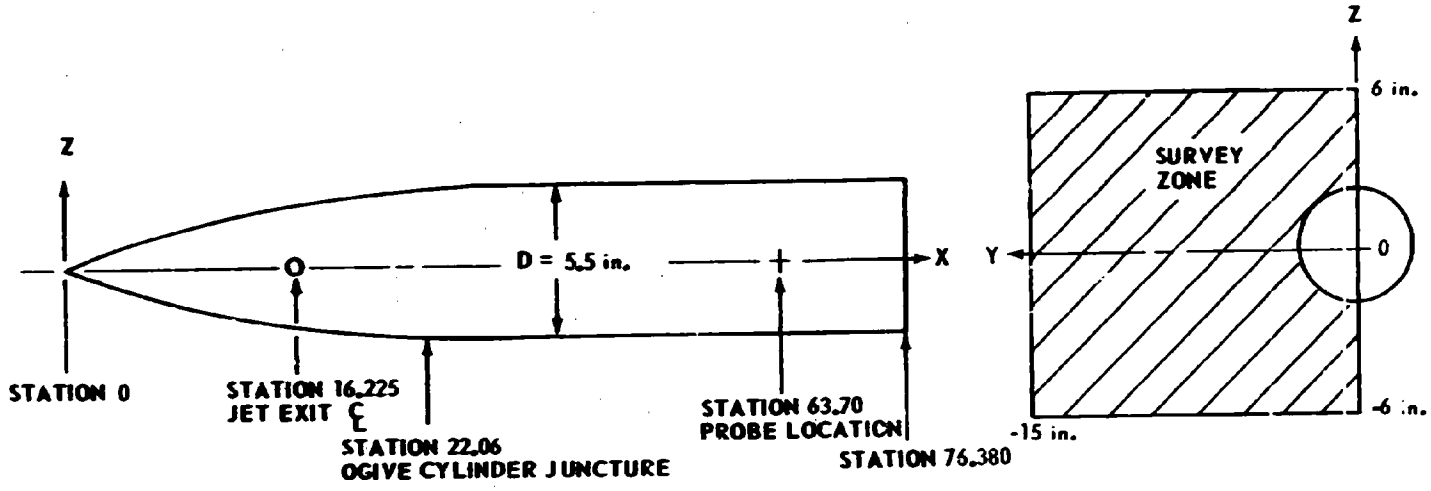

TEST SCHEDULE

M	α	P_c/P_∞	M	α	P_c/P_∞
0.9	0	10	1.2	0	10
		20			20
		40			30
		80			40
	1	20			80
	1	40			0
	3	0		1	20
	3	20			40
					80
				3	20

FIGURE 5. MODEL AND SURVEY GRID GEOMETRY

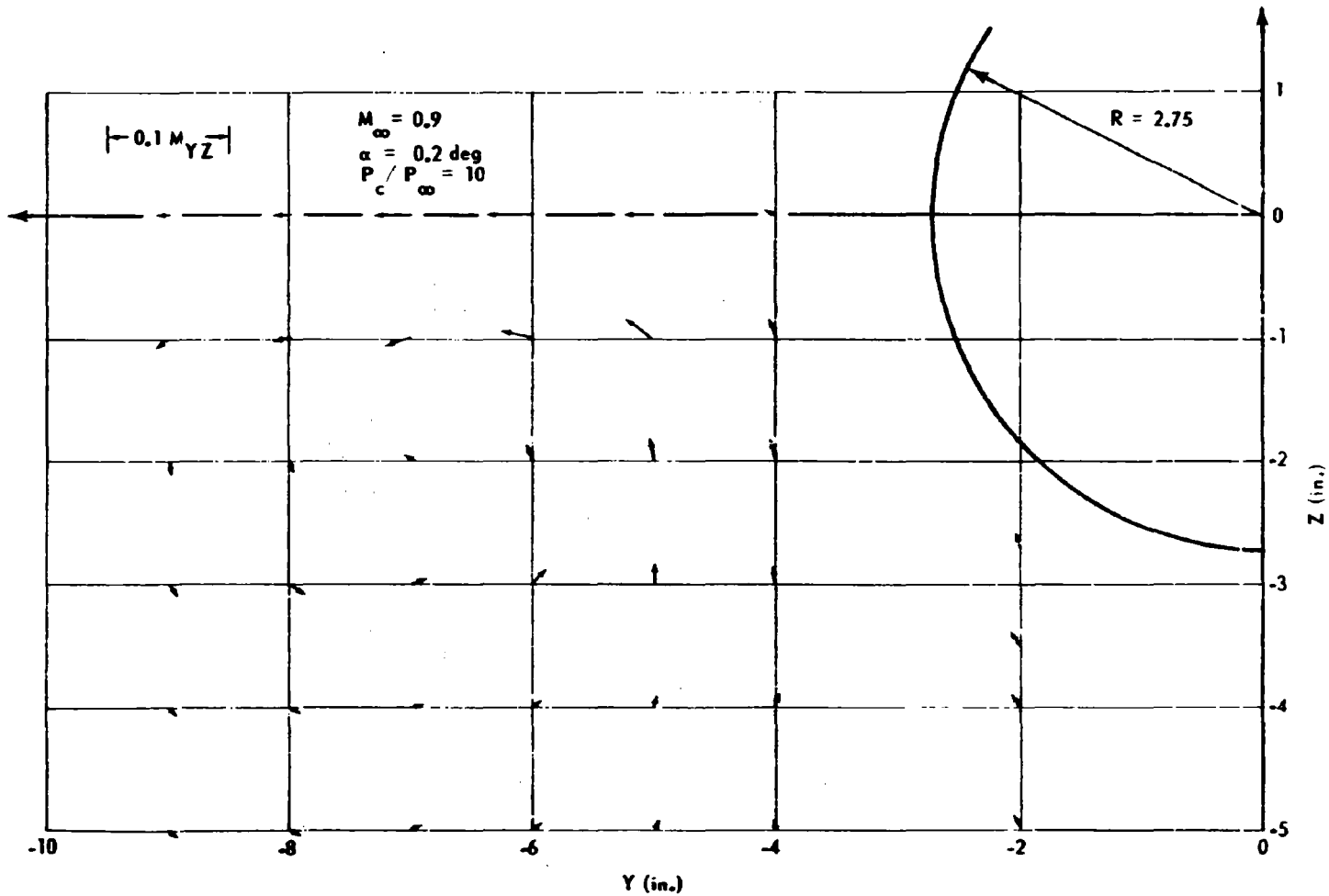

FIGURE 6. JET WAKE IN FREE STREAM FLOW FIELD AT MACH 0.9 AND ZERO ANGLE OF ATTACK

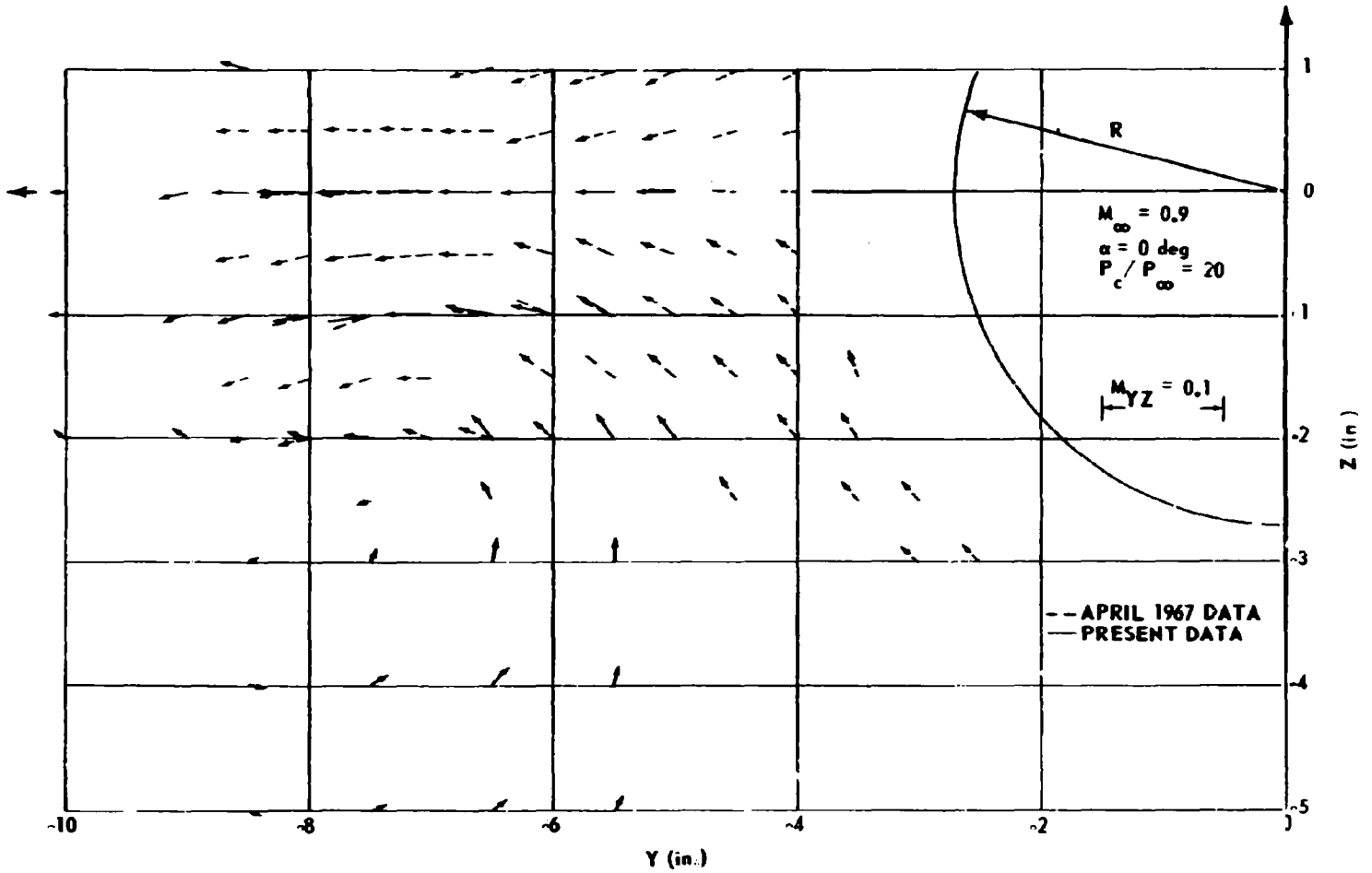

FIGURE 7. JET WAKE IN FREE STREAM FLOW FIELD AT MACH 0.9 AND ZERO ANGLE OF ATTACK

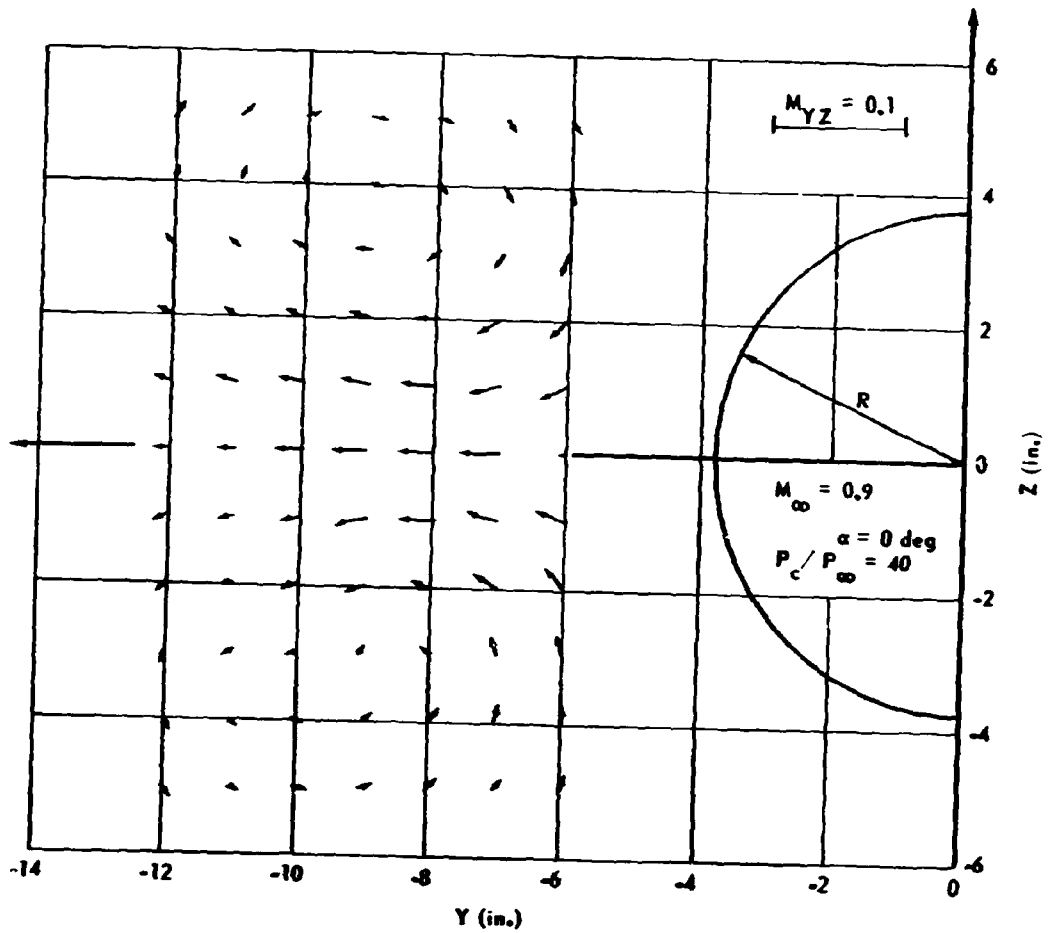

FIGURE 8. JET WAKE IN FREE STREAM FLOW FIELD AT MACH 0.9 AND ZERO ANGLE OF ATTACK

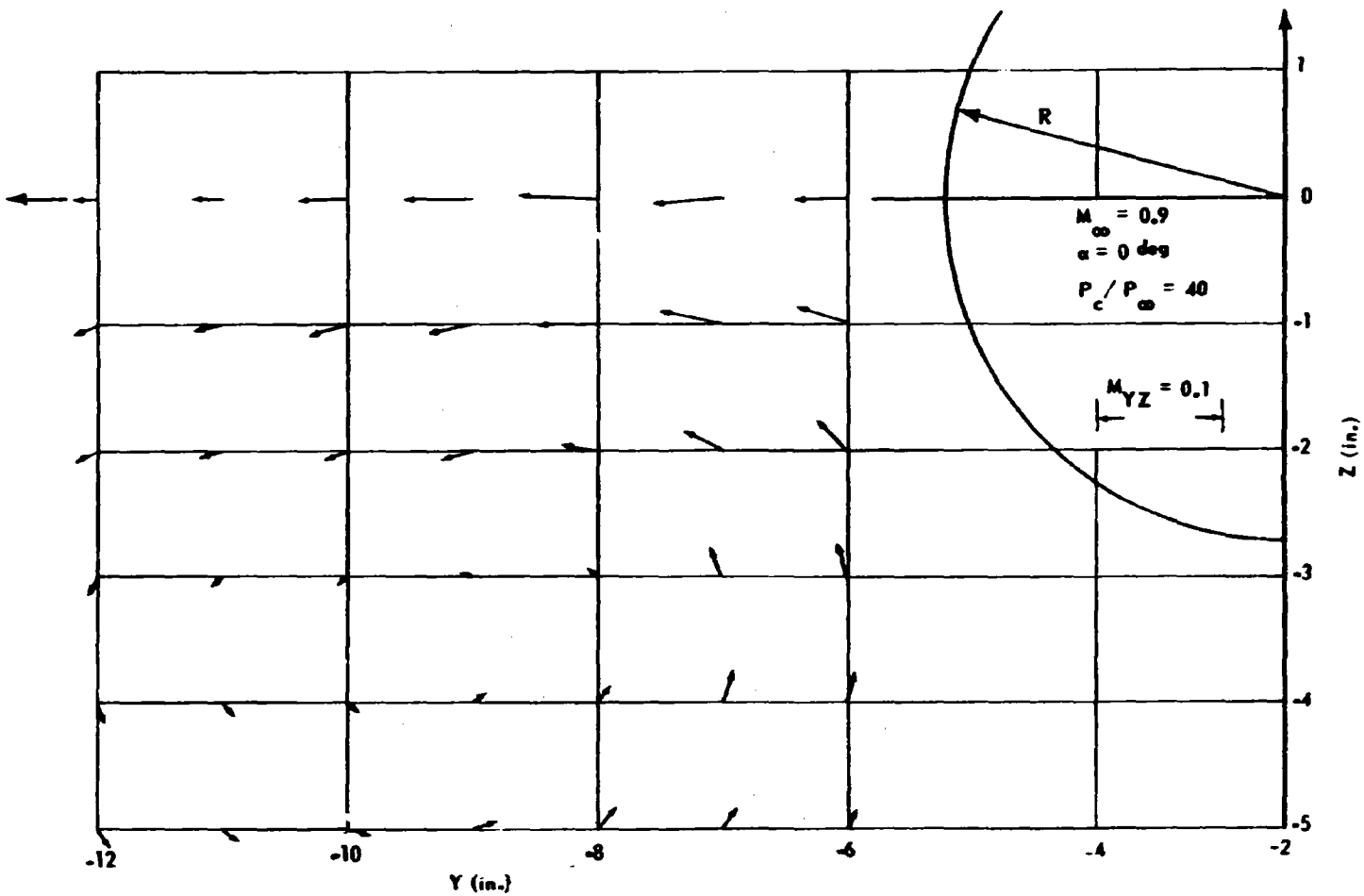

FIGURE 9. JET WAKE IN FREE STREAM FLOW FIELD AT MACH 0.9 AND ZERO ANGLE OF ATTACK

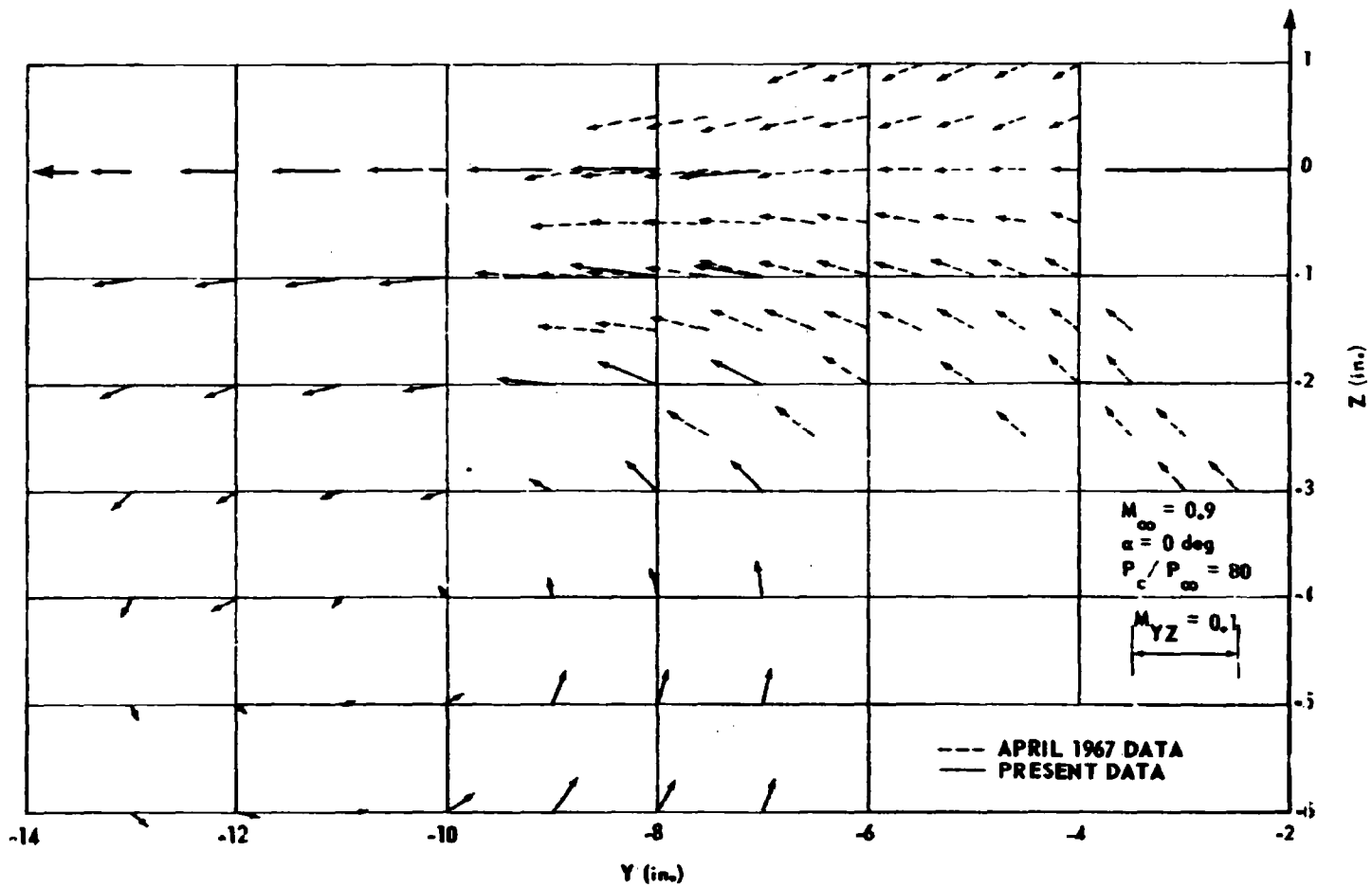

FIGURE 10. JET WAKE IN FREE STREAM FLOW FIELD AT MACH 0.9 AND ZERO ANGLE OF ATTACK

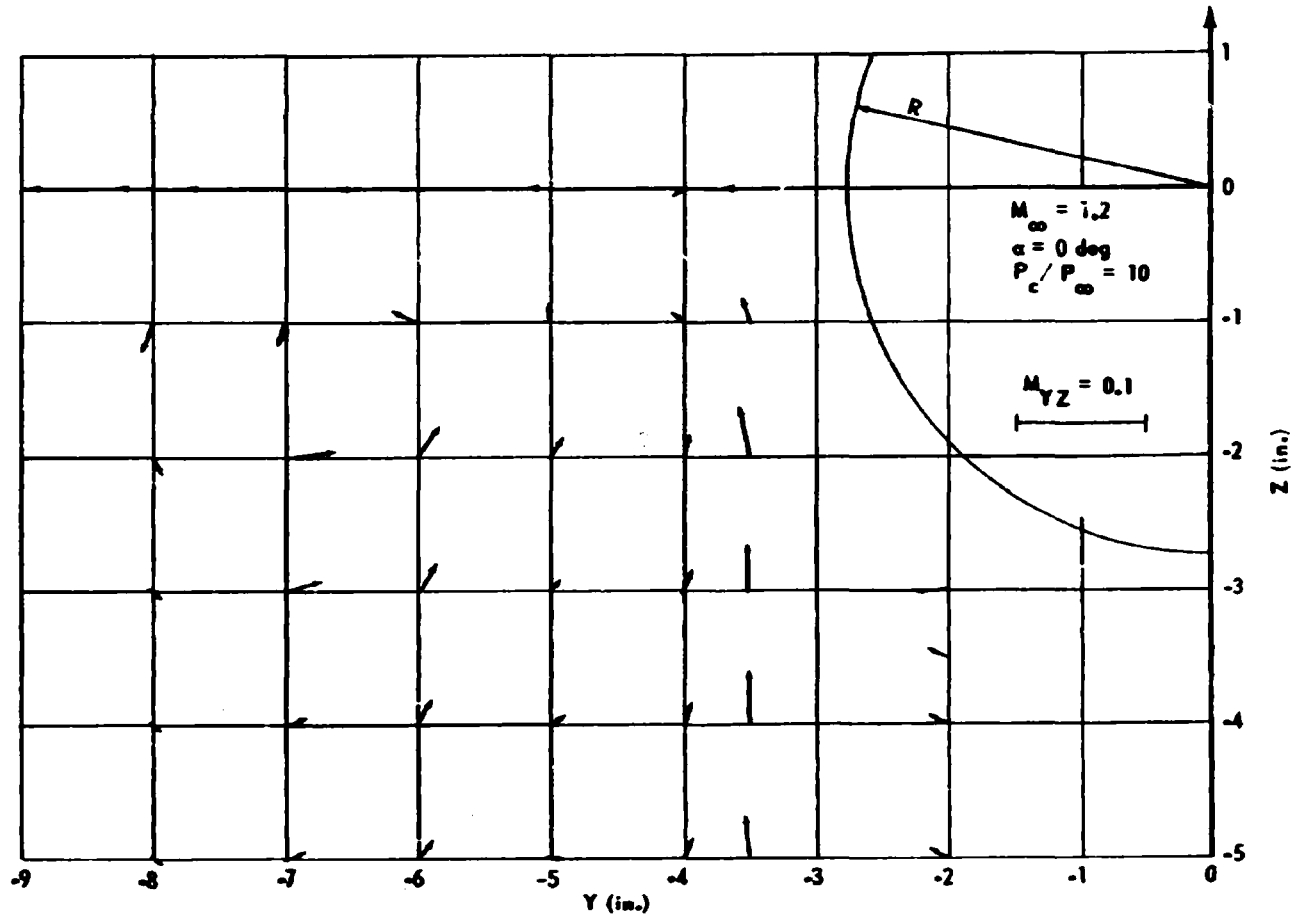

FIGURE 11. JET WAKE IN FREE STREAM FLOW FIELD AT MACH 1.2 AND ZERO ANGLE OF ATTACK

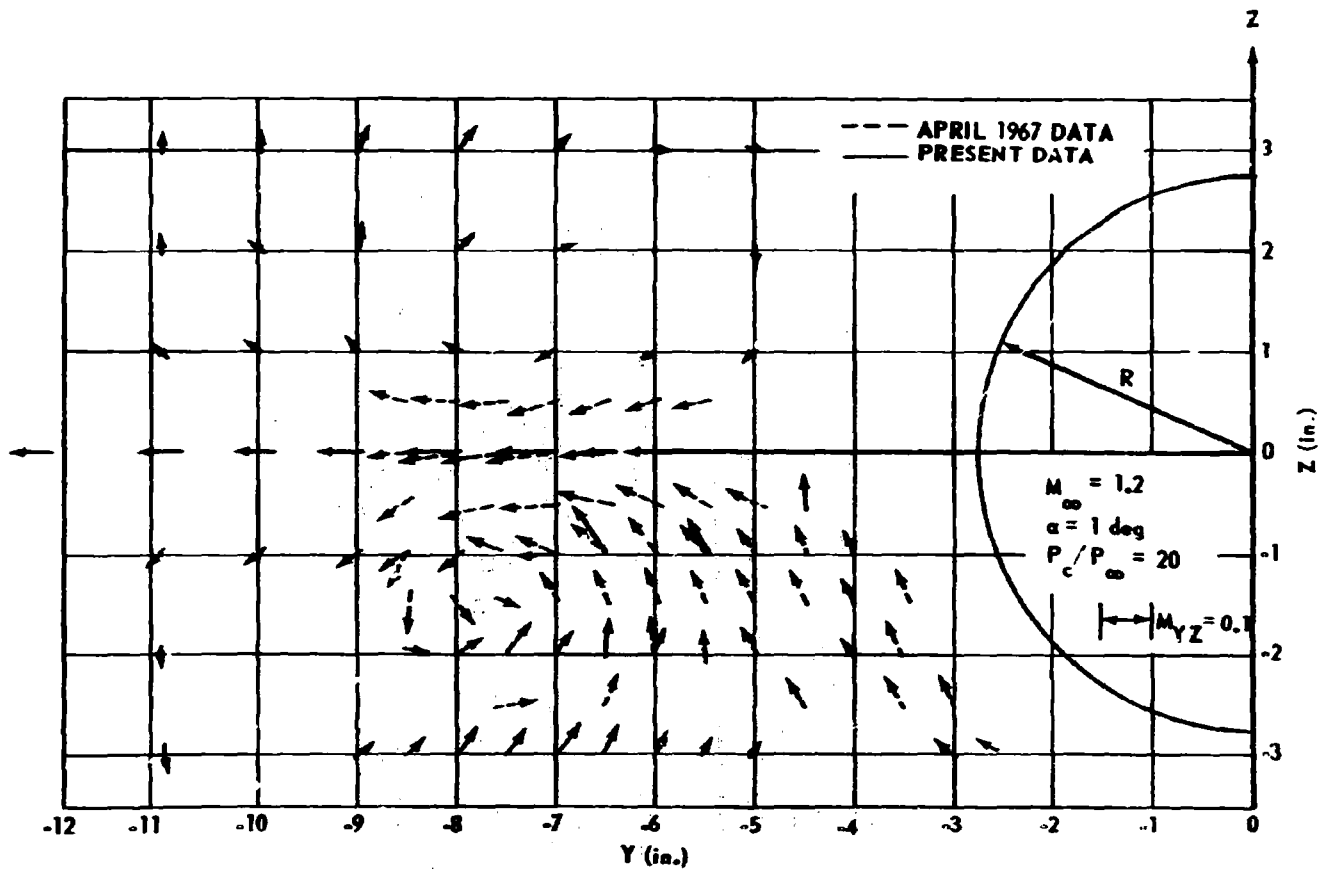

FIGURE 12. JET WAKE IN FREE STREAM FLOW FIELD AT MACH 1.2 AND ZERO ANGLE OF ATTACK

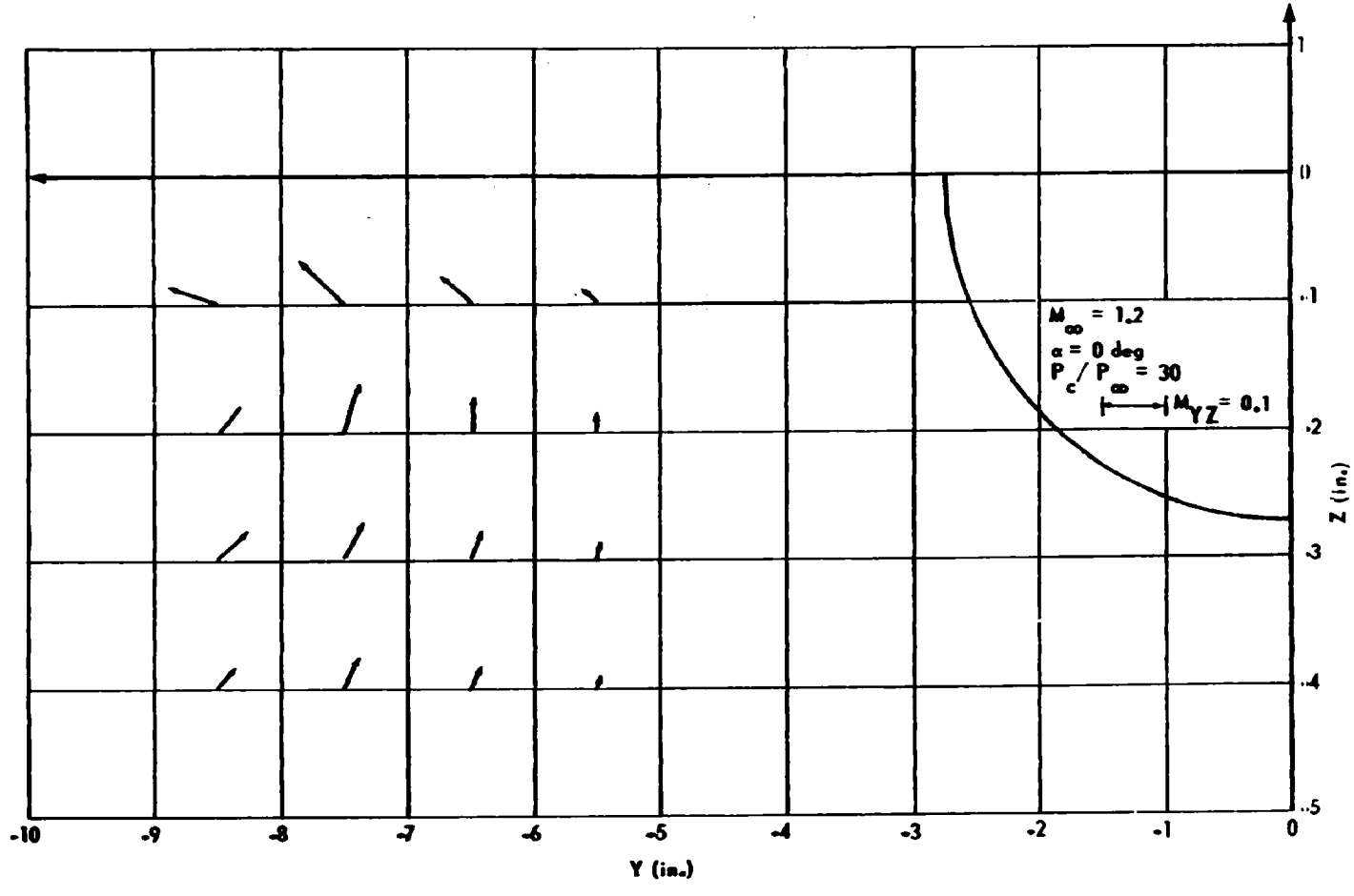

FIGURE 13. JET WAKE IN FREE STREAM FLOW FIELD AT MACH 1.2 AND ZERO ANGLE OF ATTACK

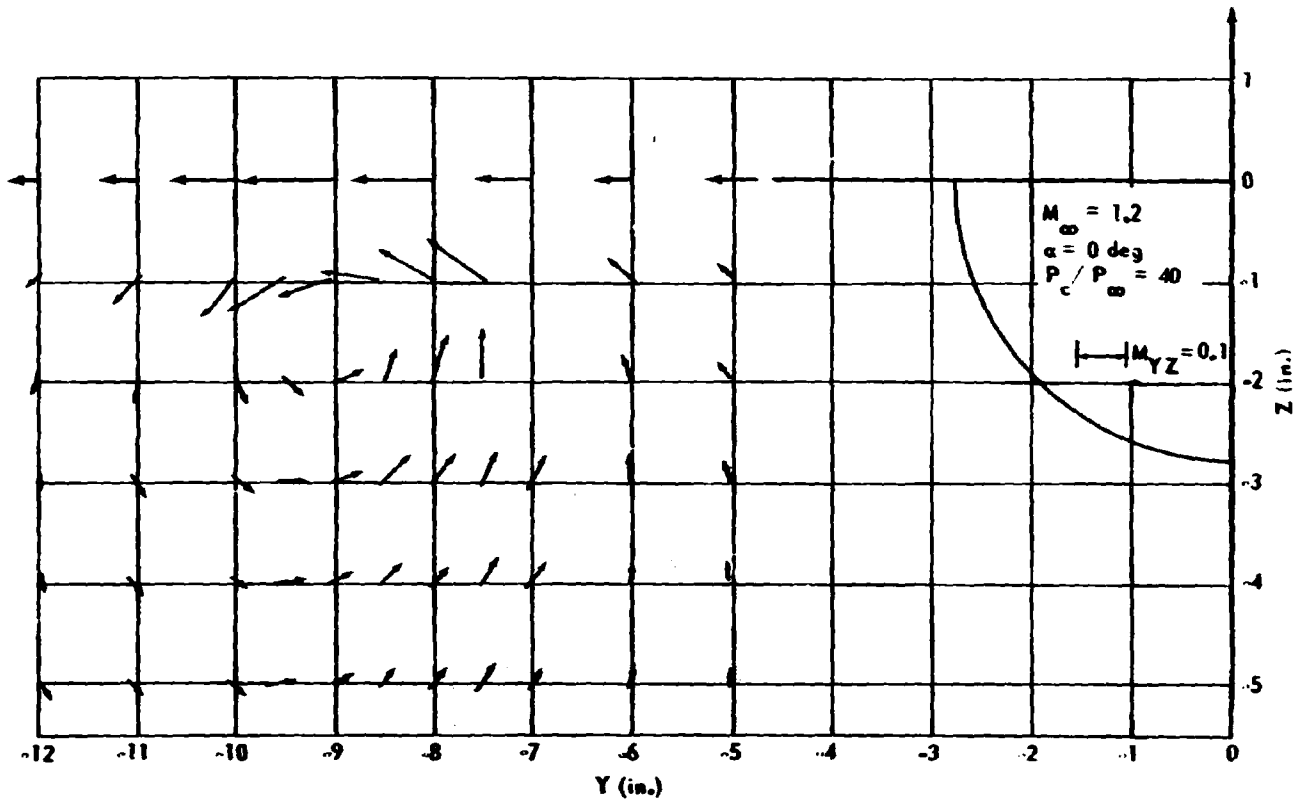

FIGURE 14. JET WAKE IN FREE STREAM FLOW FIELD AT MACH 1.2 AND ZERO ANGLE OF ATTACK

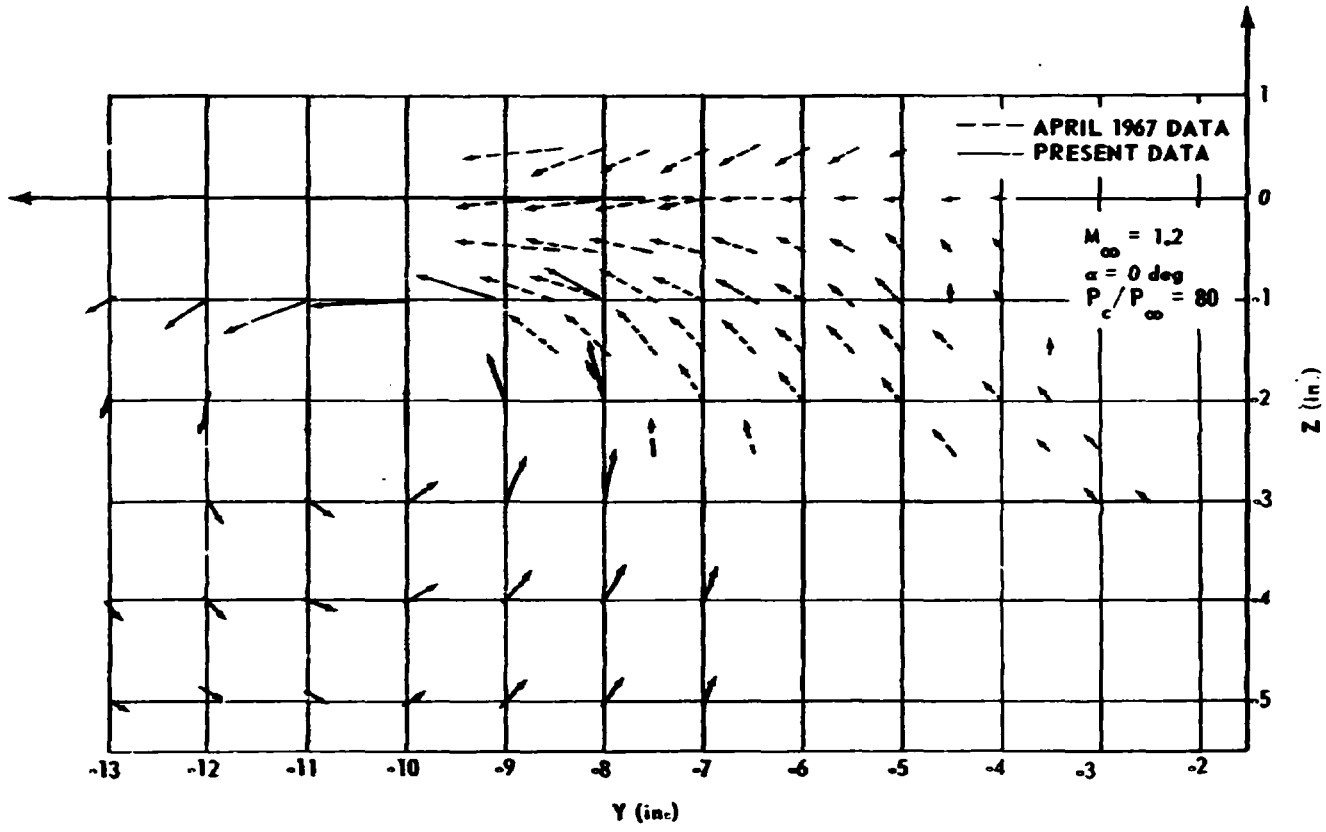

FIGURE 15. JET WAKE IN FREE STREAM FLOW FIELD AT MACH 1.2 AND ZERO ANGLE OF ATTACK

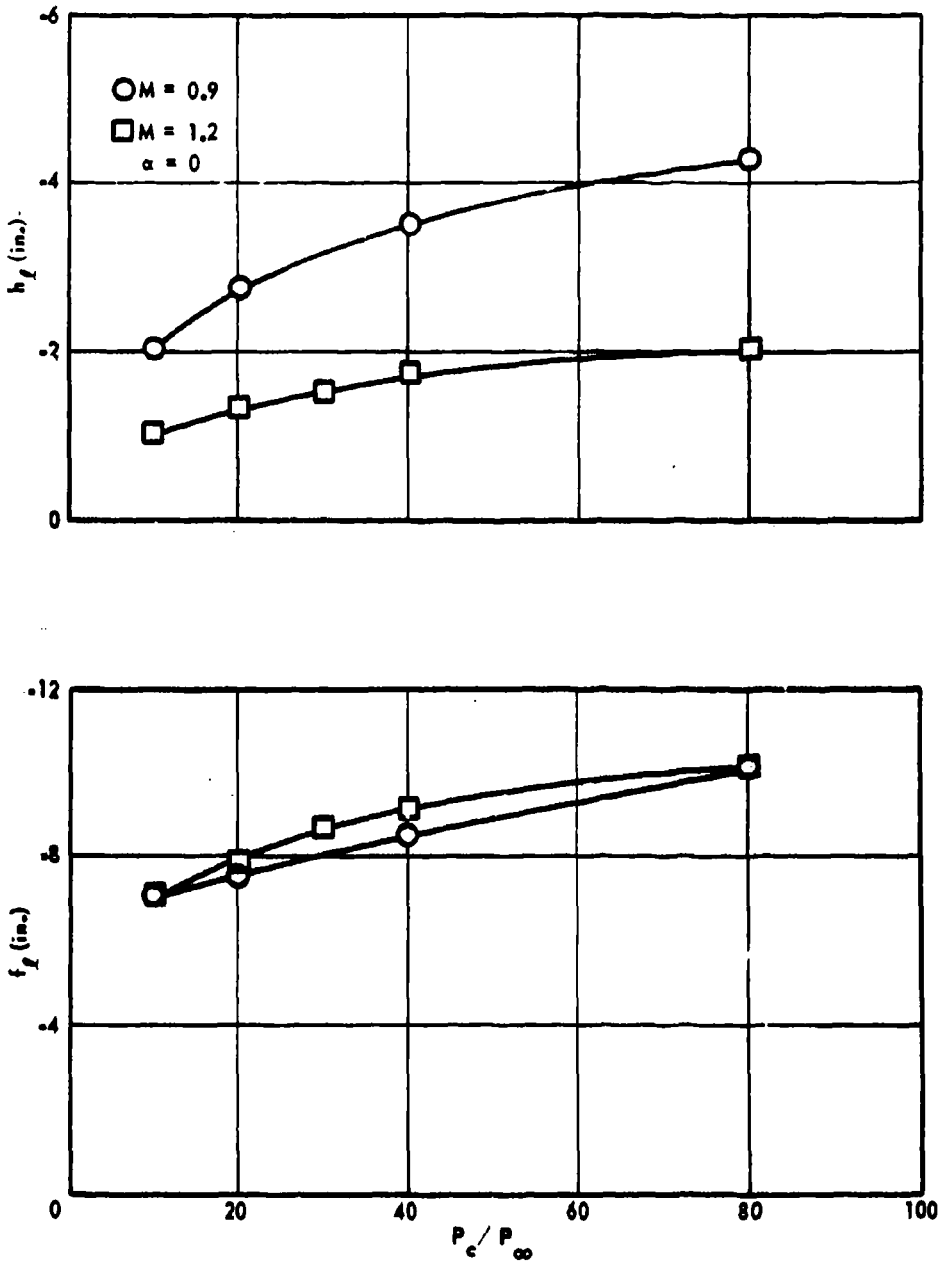

FIGURE 16. LOWER VORTEX CORE COORDINATES

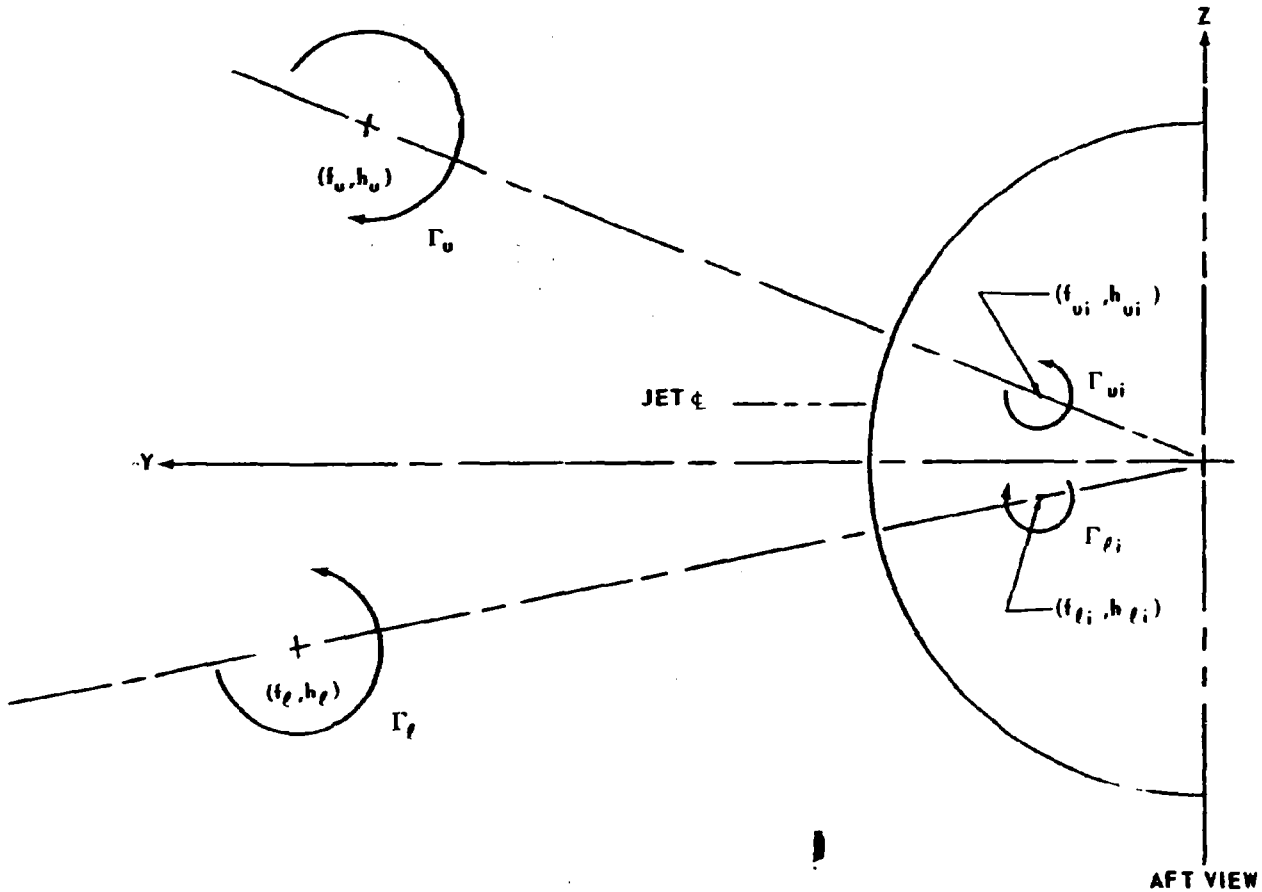

FIGURE 17. VORTEX PATTERN

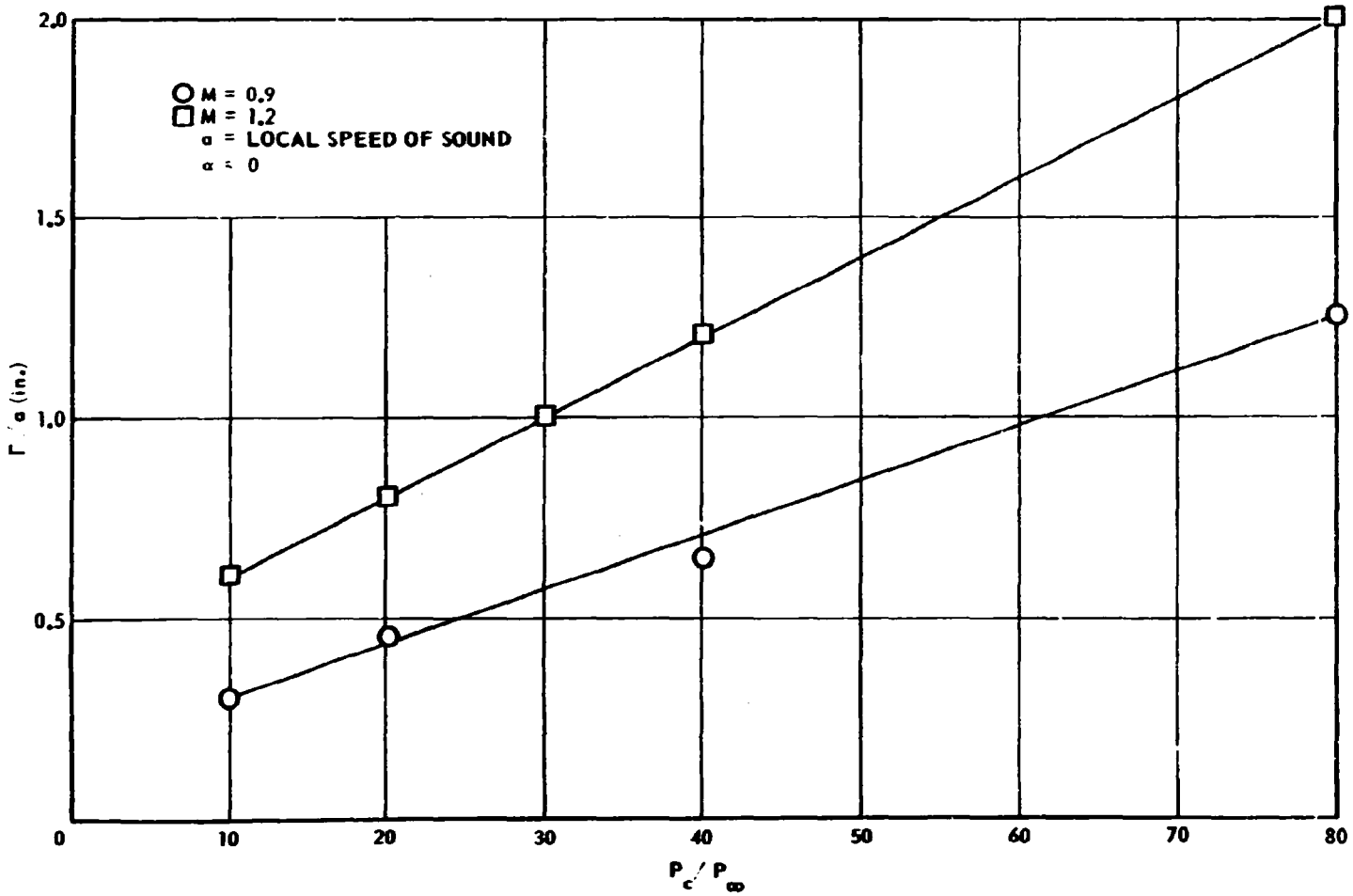

FIGURE 18. VORTEX STRENGTHS

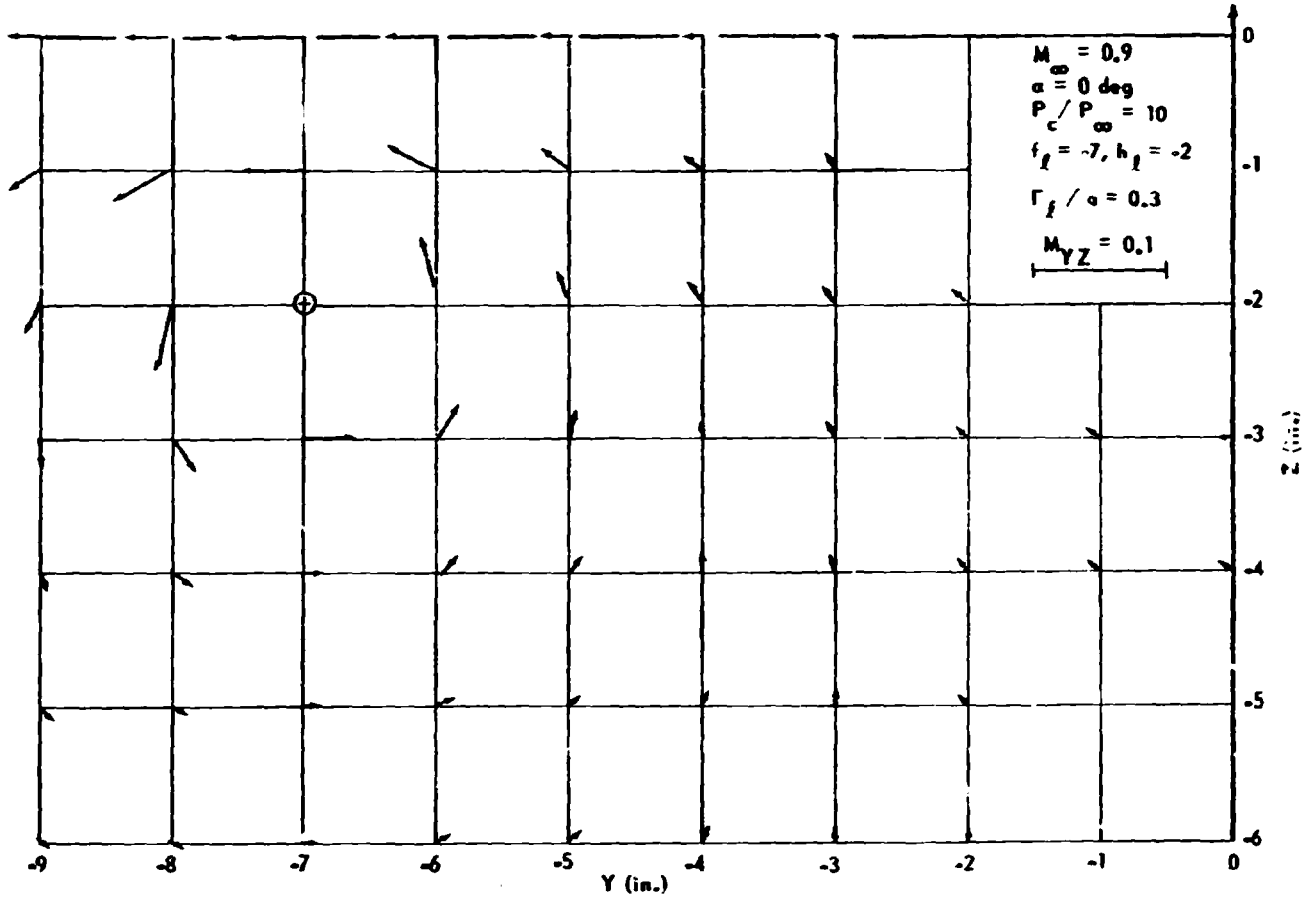

FIGURE 19. COMPUTED FLOW FIELD FOR MACH 0.9 AND α = 0 DEGREE

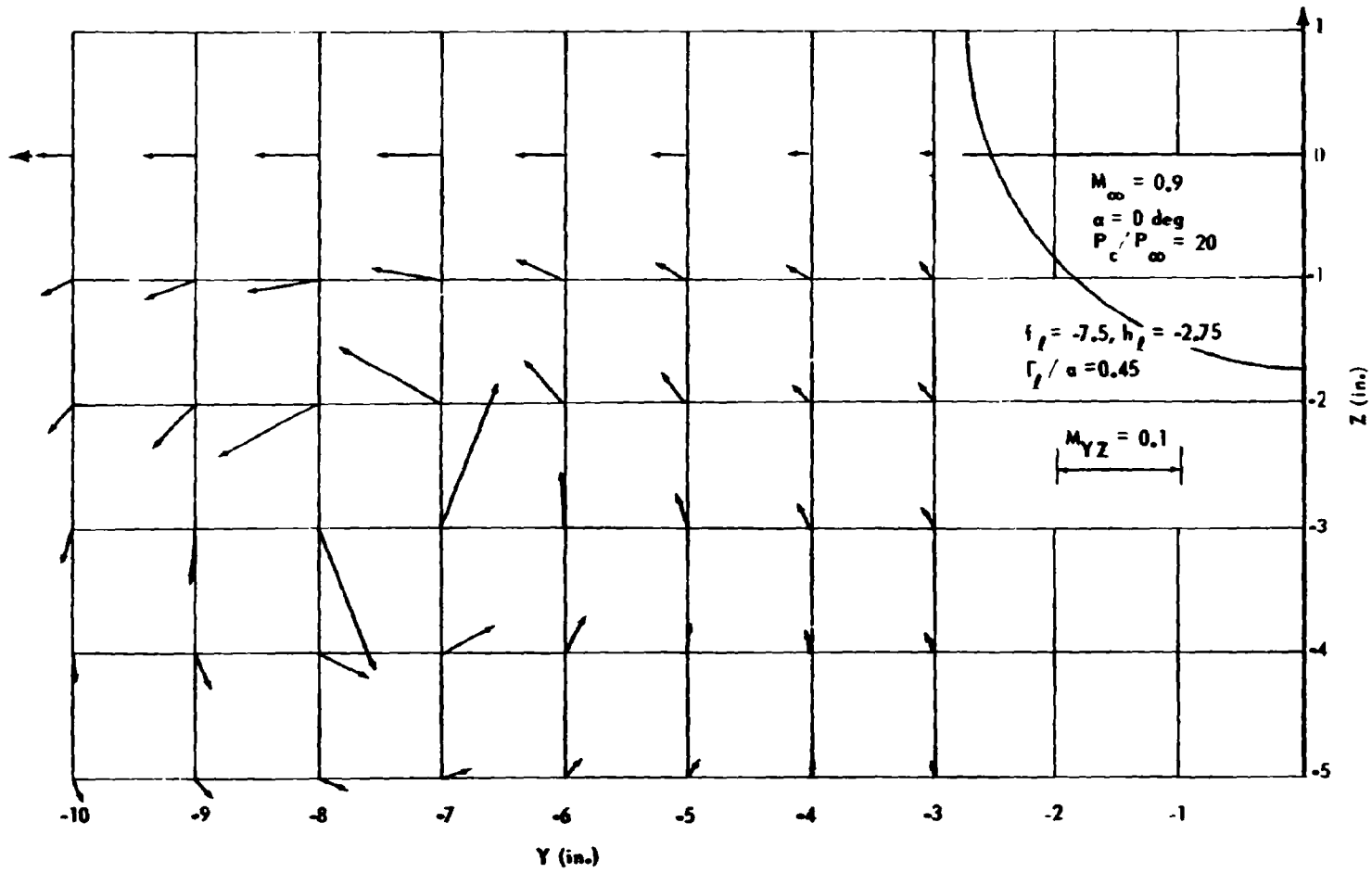

FIGURE 20. COMPUTED FLOW FIELD FOR MACH 0.9 AND α = 0 DEGREE

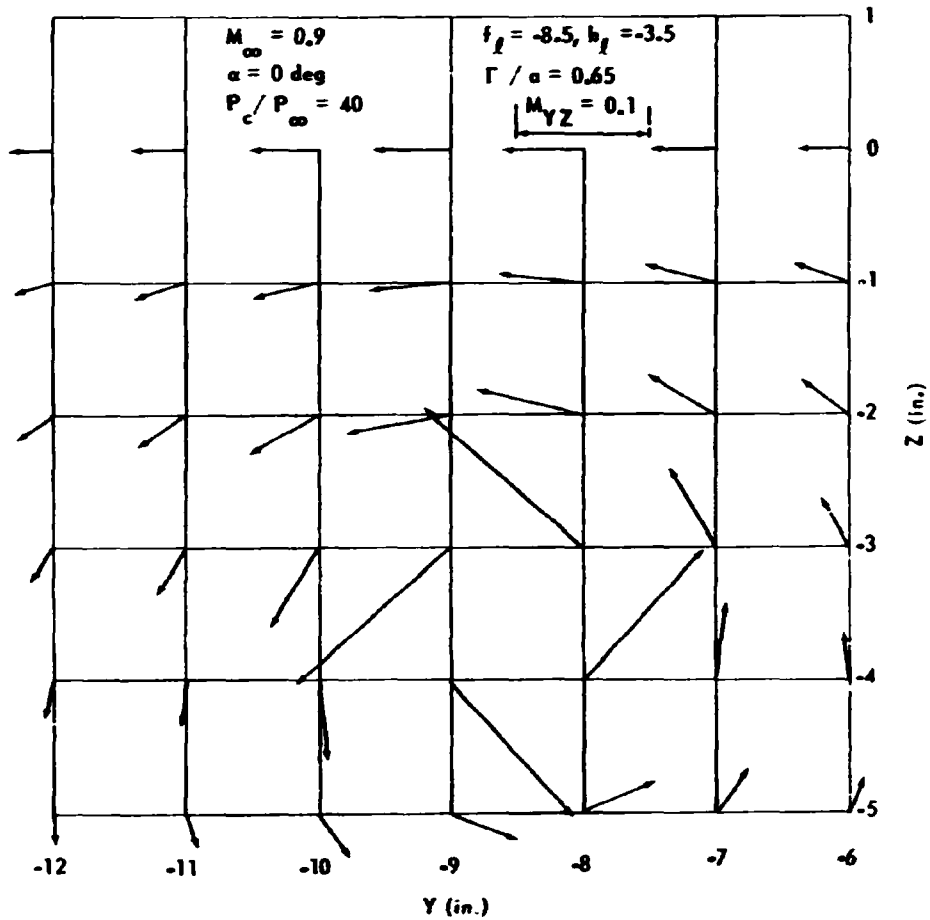

FIGURE 21. COMPUTED FLOW FIELD FOR MACH 0.9 AND α 0 DEGREE

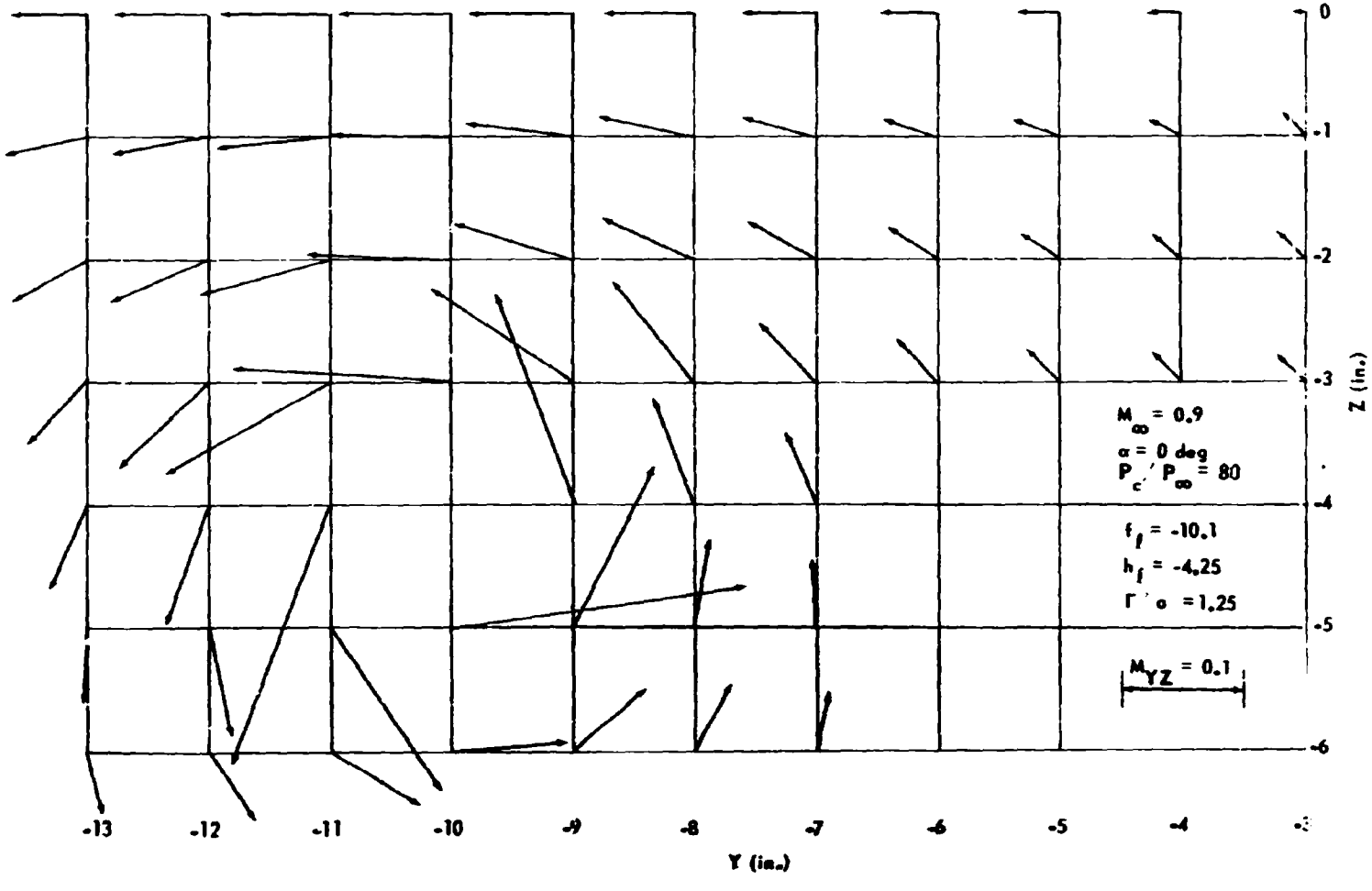

FIGURE 22. COMPUTED FLOW FIELD FOR MACH 0.9 AND α = 0 DEGREE

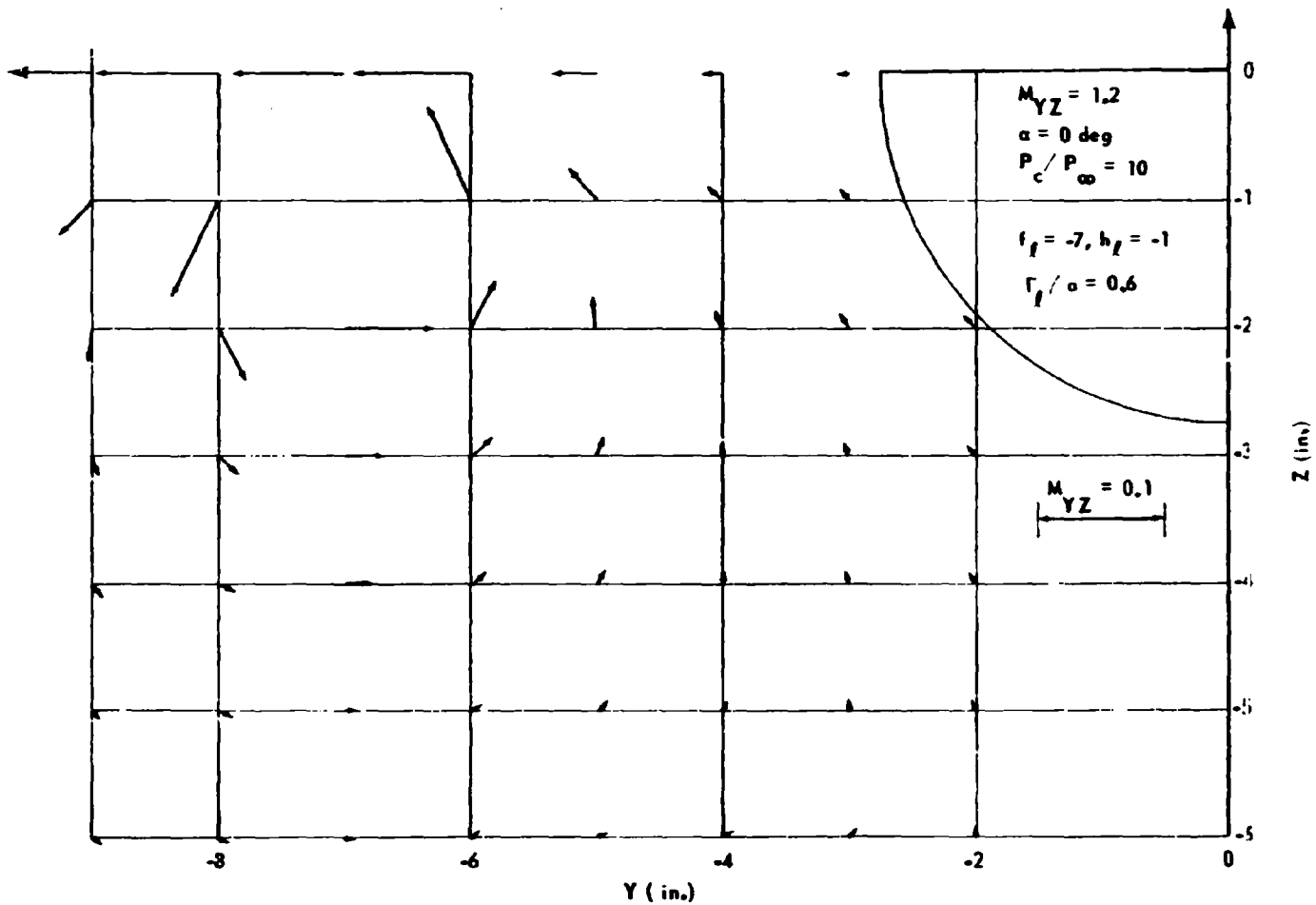

FIGURE 23. COMPUTED FLOW FIELD FOR MACH 1.2 AND α = 0 DEGREE

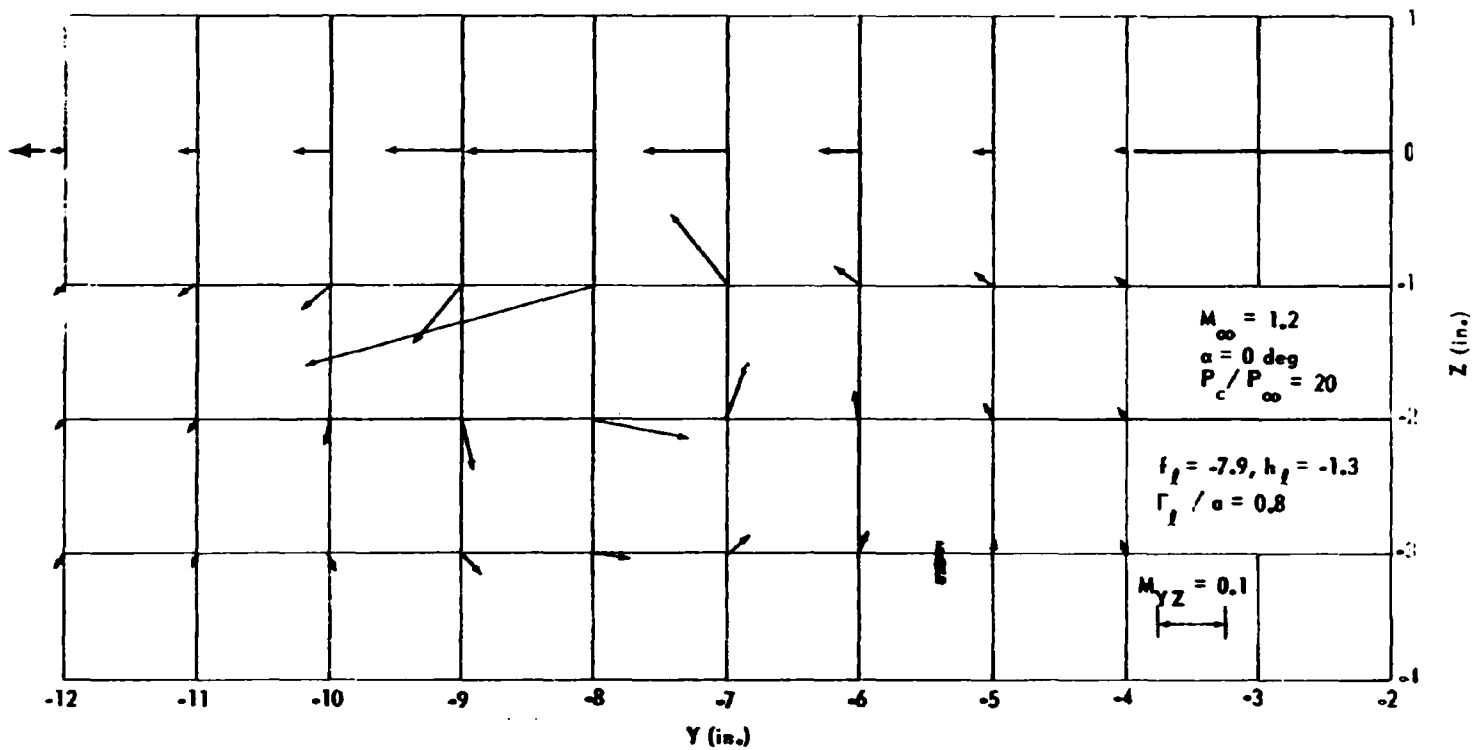

FIGURE 24. COMPUTED FLOW FIELD FOR MACH 1.2 AND α = 0 DEGREE

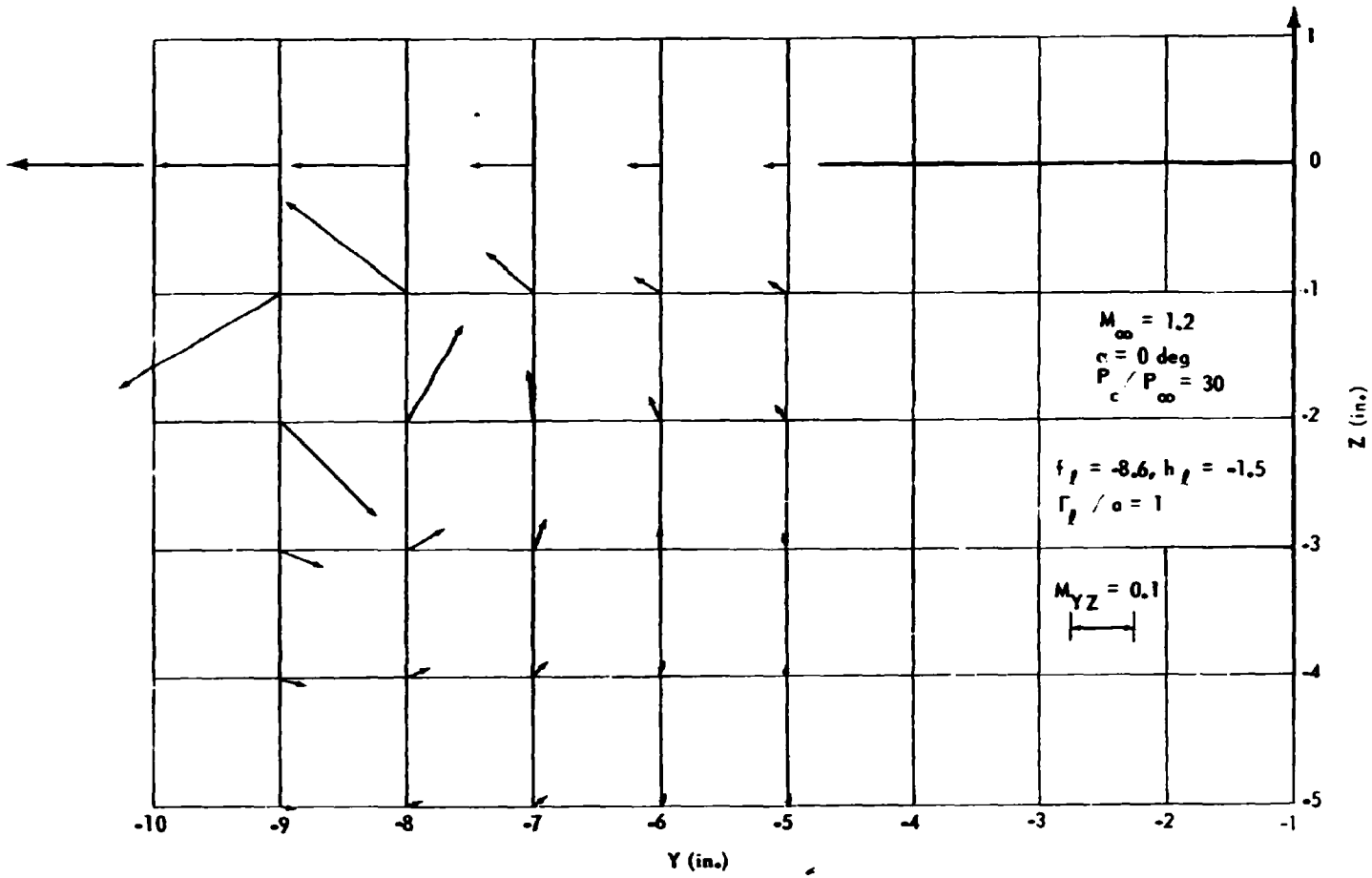

FIGURE 25. COMPUTED FLOW FIELD FOR MACH 1.2 AND α = 0 DEGREE

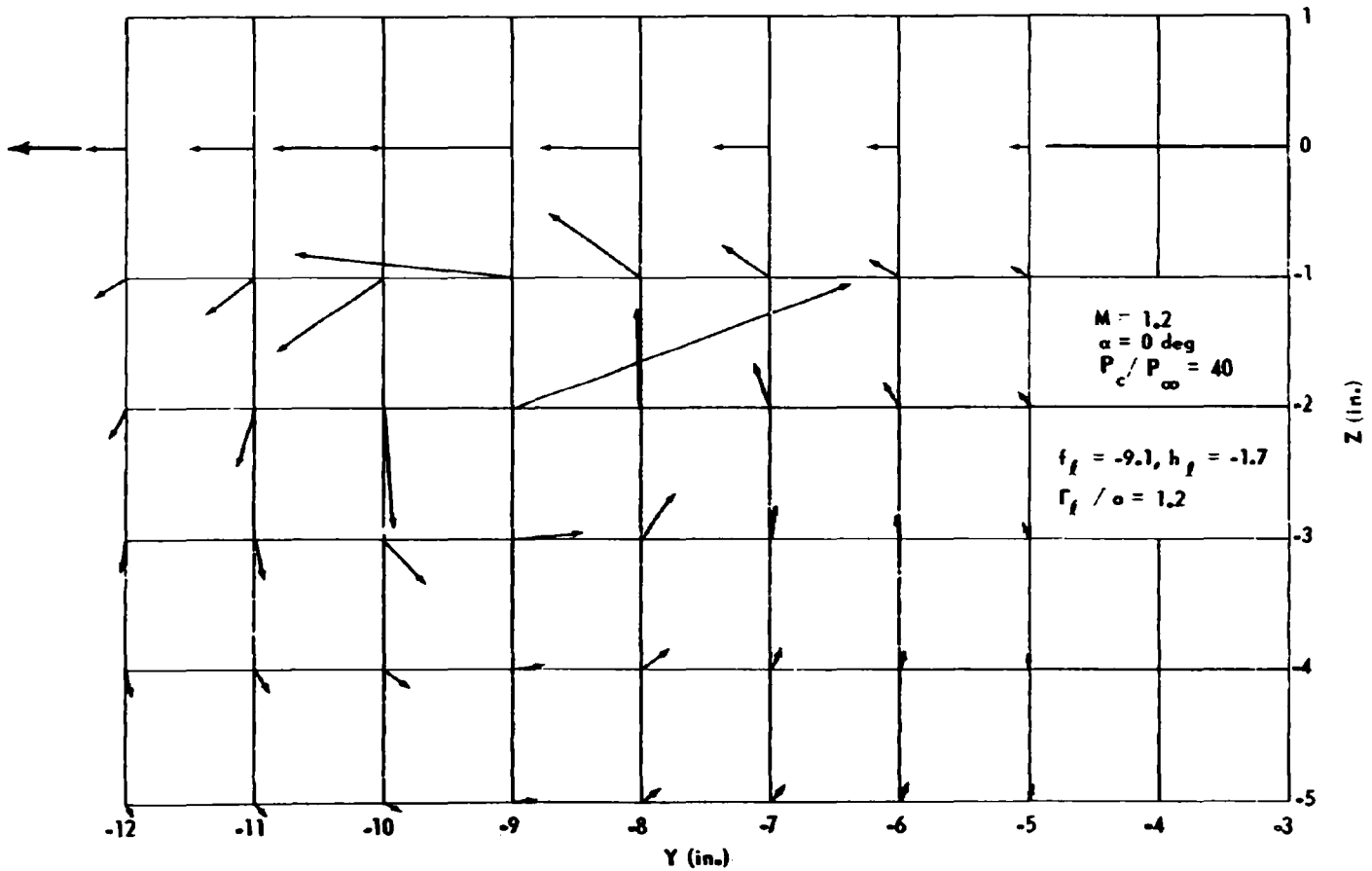

FIGURE 26. COMPUTED FLOW FIELD FOR MACH 1.2 AND α = 0 DEGREE

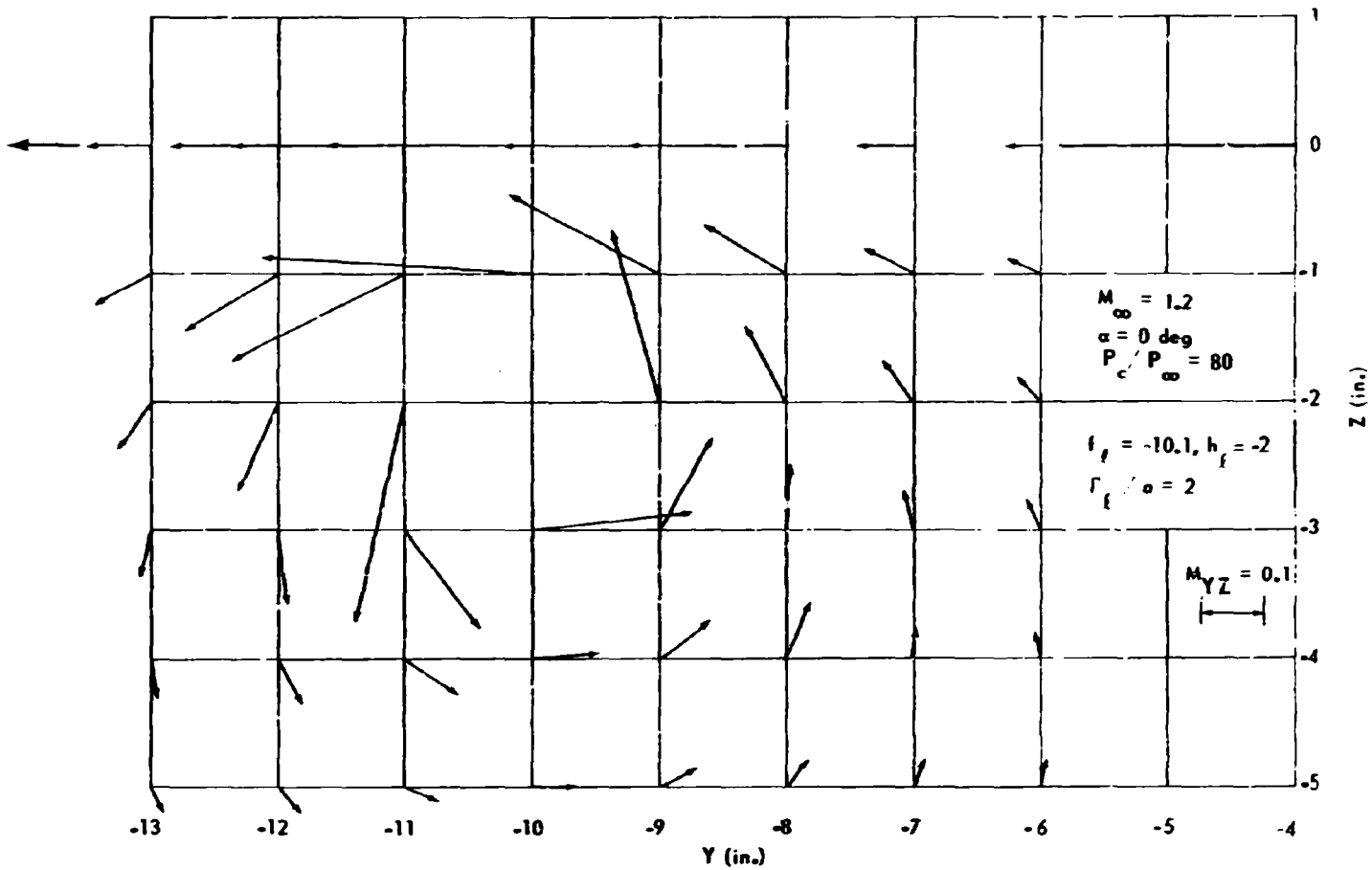

FIGURE 27. COMPUTED FLOW FIELD FOR MACH 1.2 AND α = 0 DEGREE

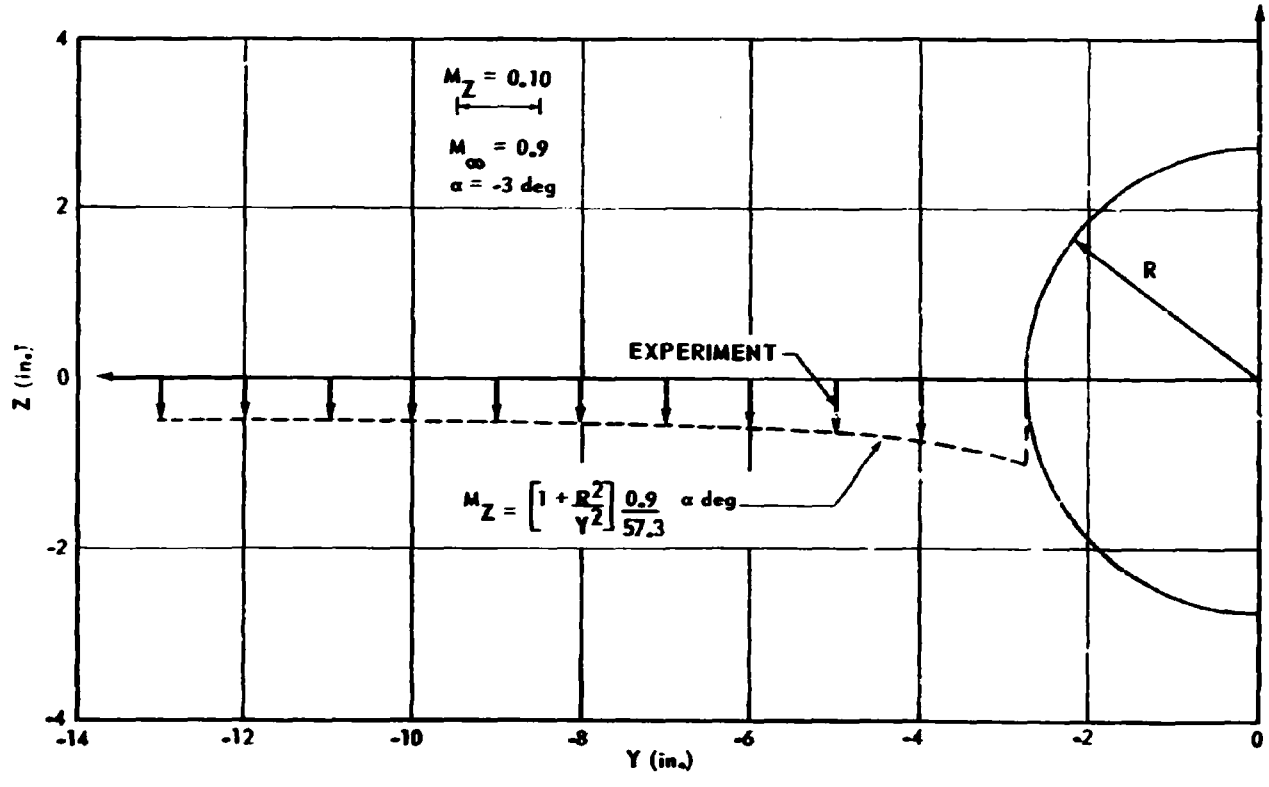

FIGURE 28. FLOW-FIELD THEORY UPWASH COMPARISONS

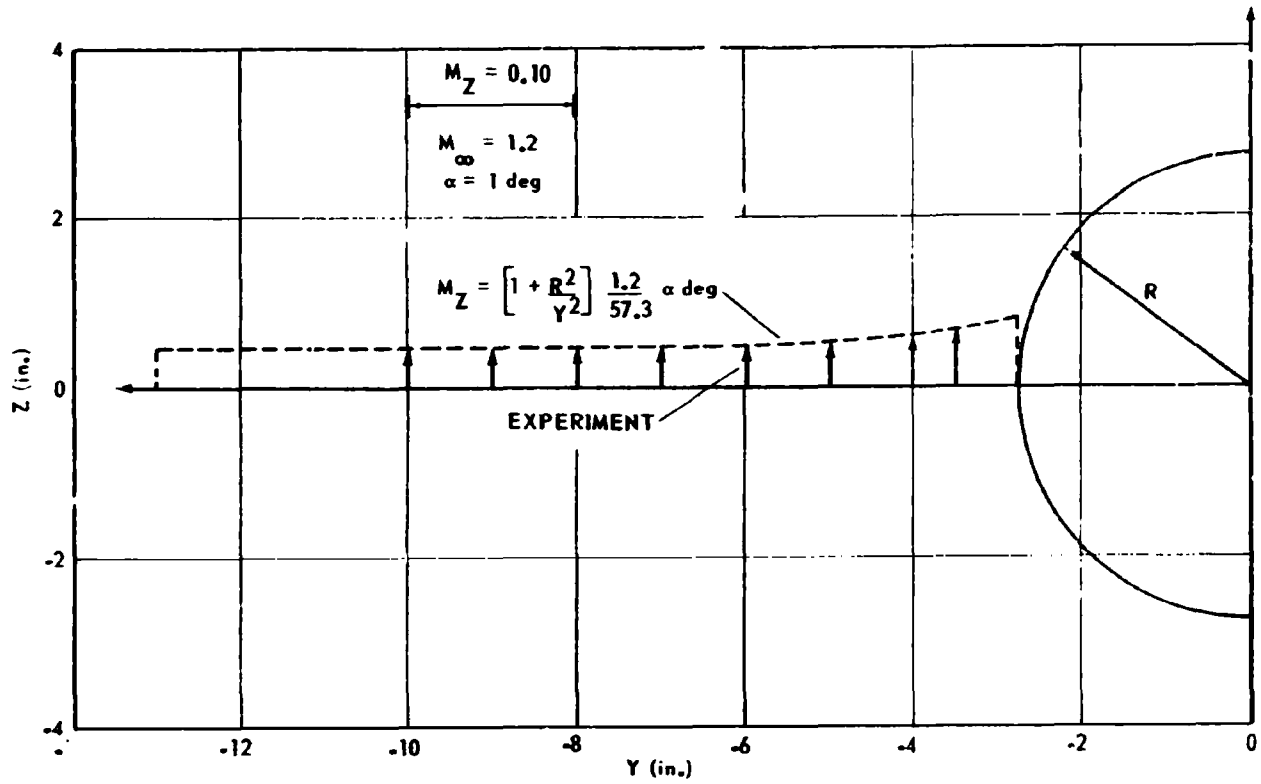

FIGURE 29. FLOW-FIELD THEORY UPWASH COMPARISONS

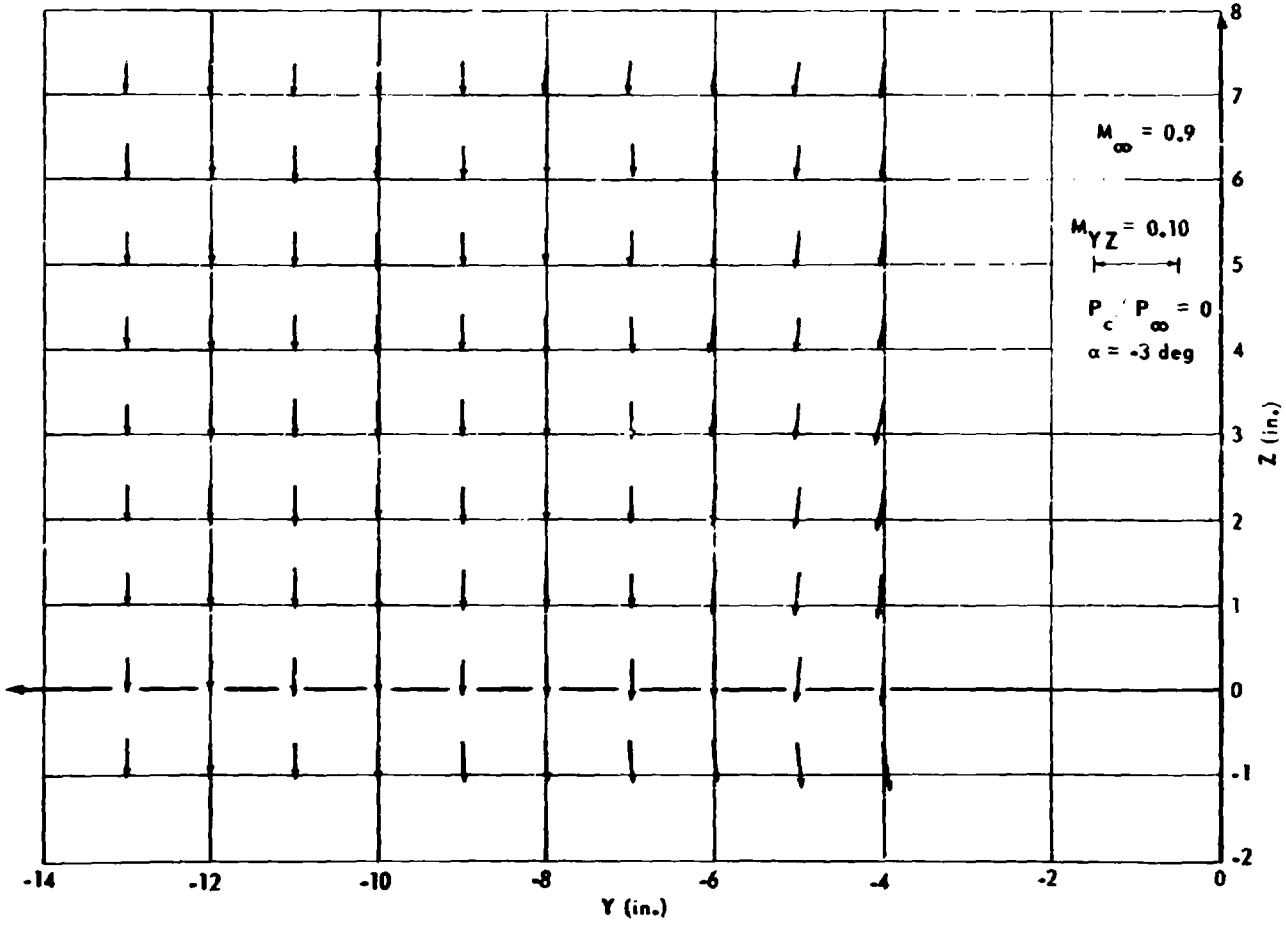

FIGURE 30. FREE STREAM FLOW FIELD

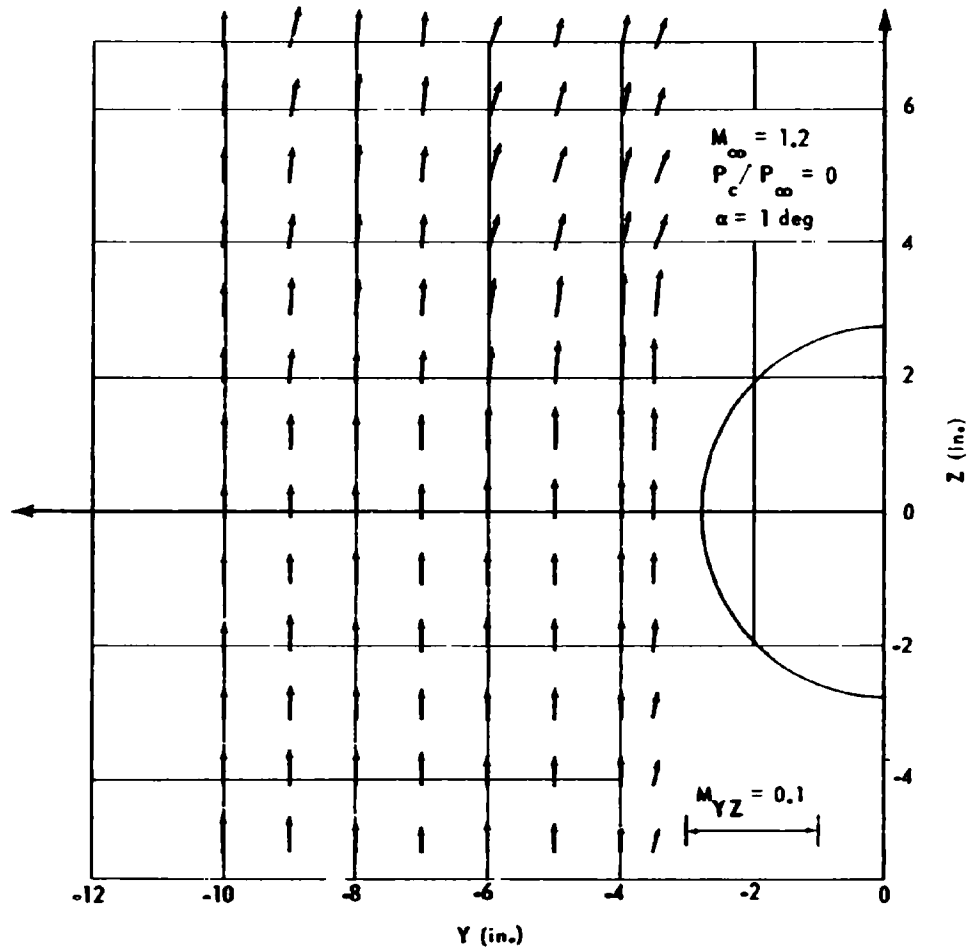

FIGURE 31. FREE STREAM FLOW FIELD

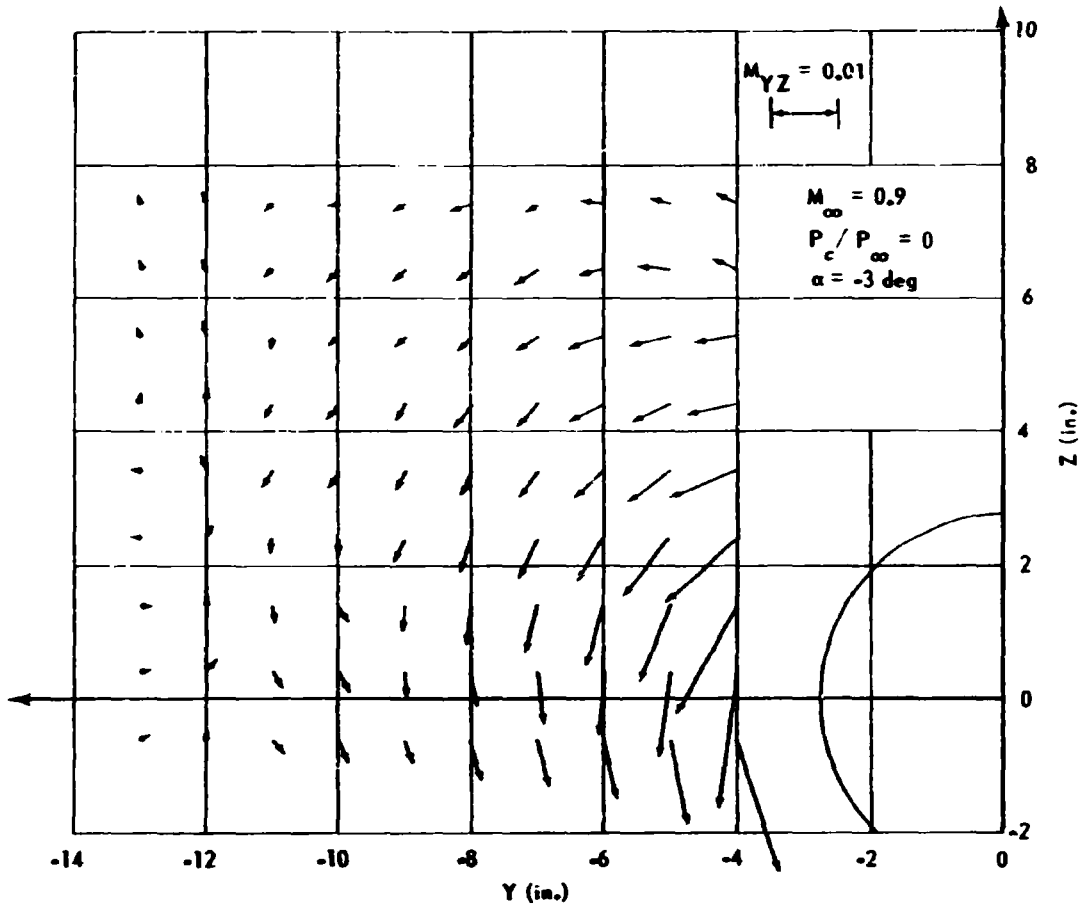

FIGURE 32. PERTURBATION OF FREE STREAM FLOW FIELD

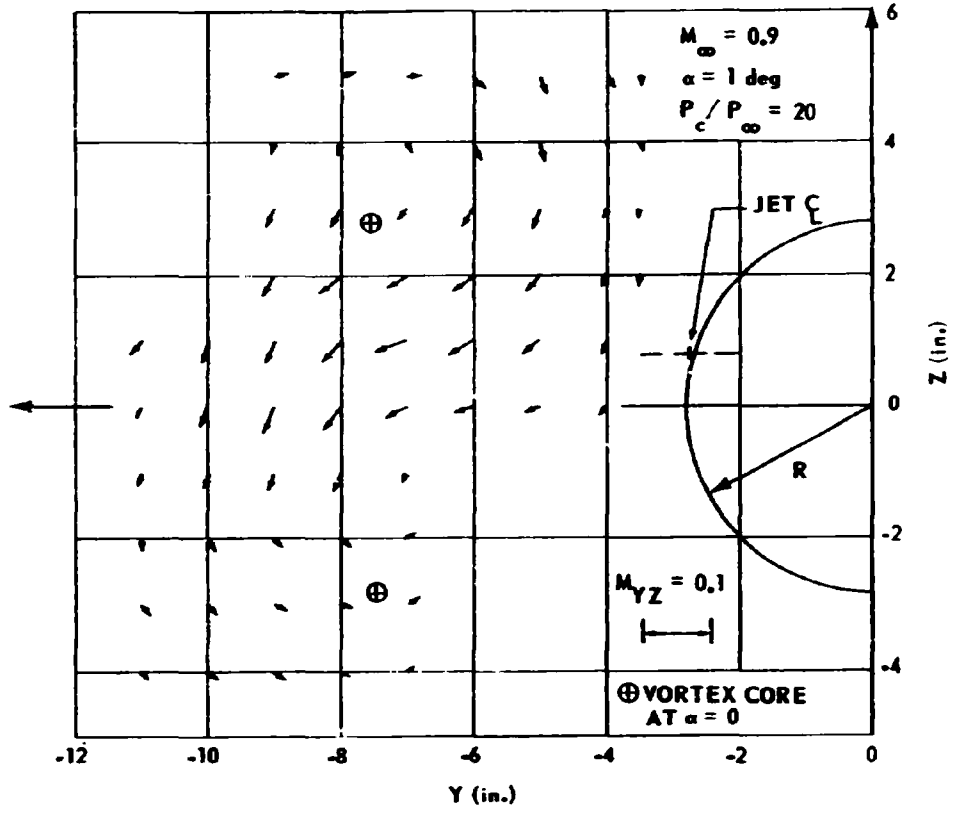

FIGURE 33. PERTURBATION OF FREE STREAM FLOW FIELD DUE TO JET WAKE AND ANGLE OF ATTACK

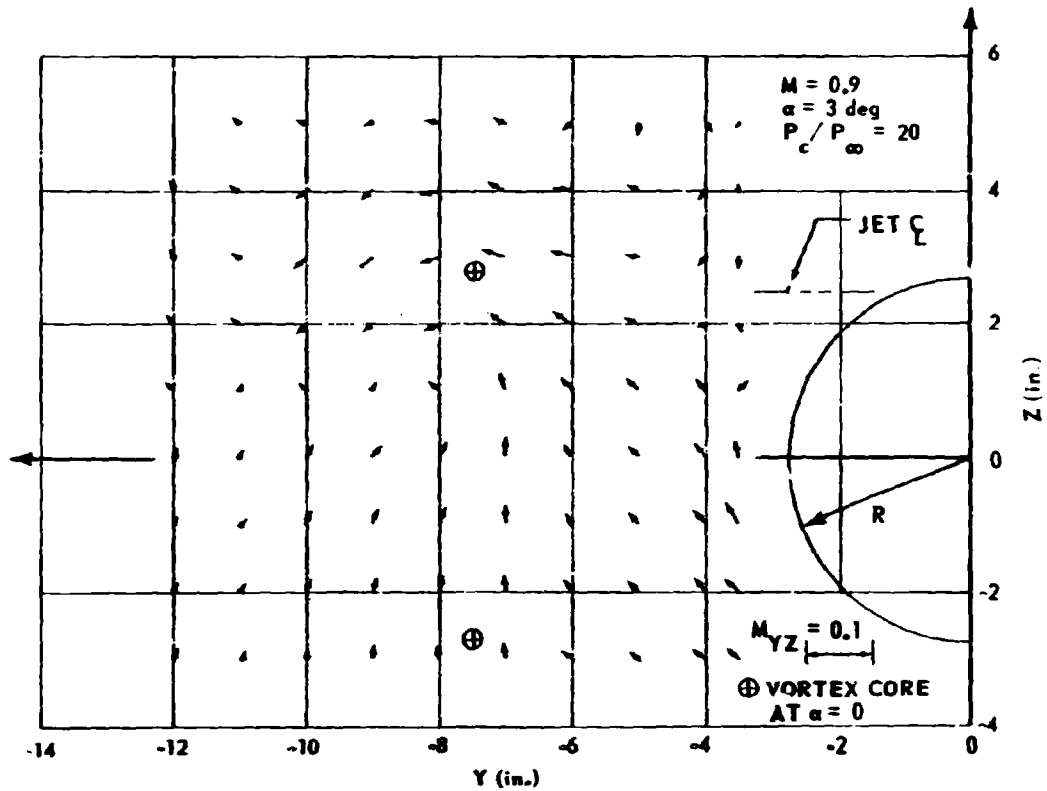

FIGURE 34. PERTURBATION OF FREE STREAM FLOW FIELD DUE TO JET WAKE AND ANGLE OF ATTACK

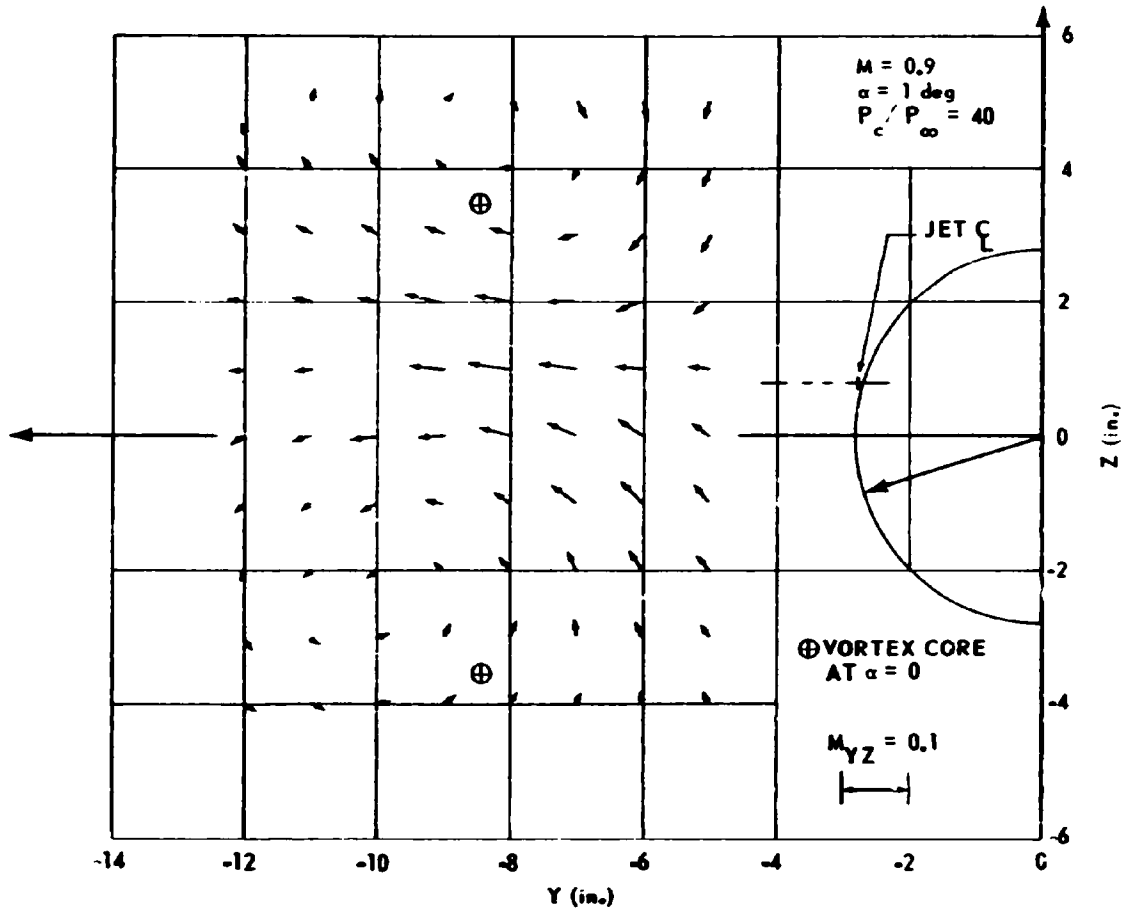

FIGURE 35. PERTURBATION OF FREE STREAM FLOW FIELD DUE TO JET WAKE AND ANGLE OF ATTACK

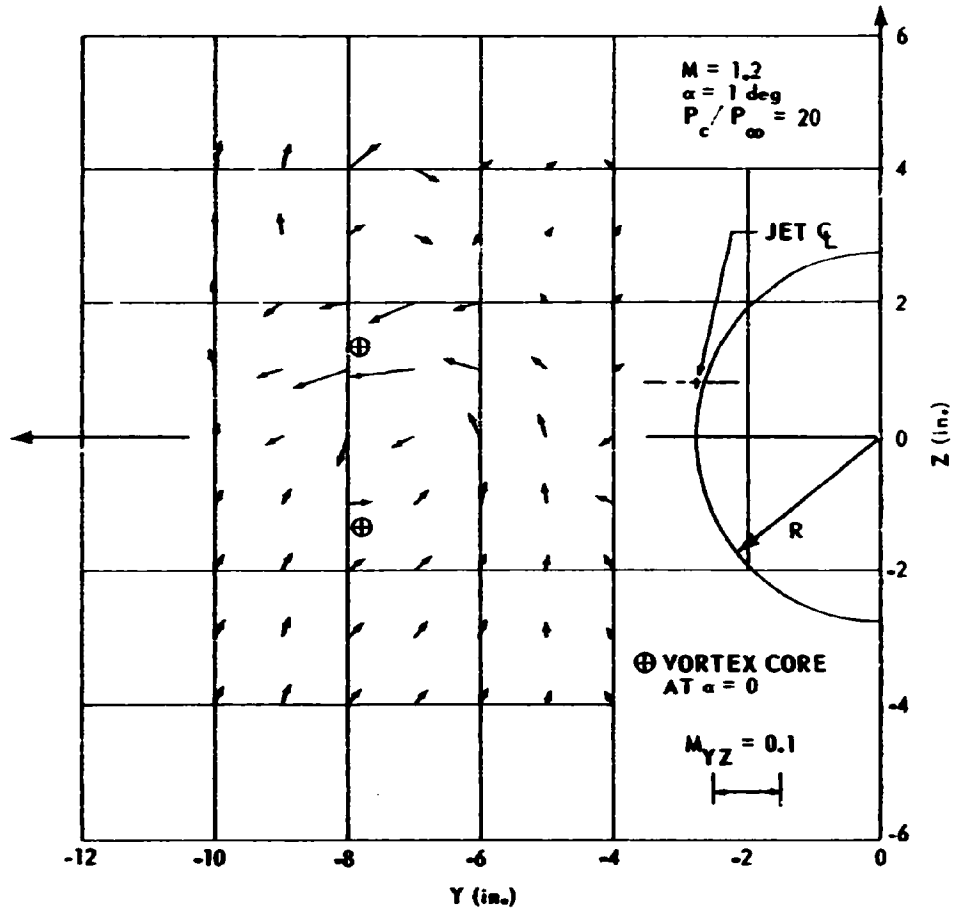

FIGURE 36. PERTURBATION OF FREE STREAM FLOW FIELD DUE TO JET WAKE AND ANGLE OF ATTACK

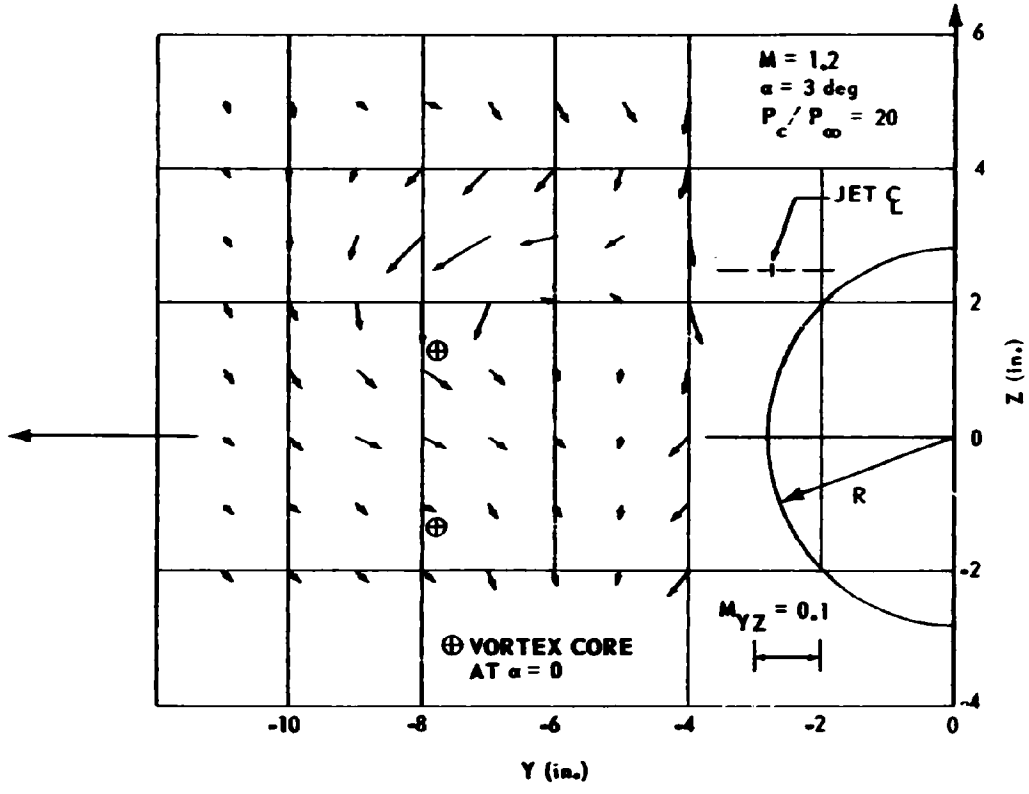

FIGURE 37. PERTURBATION OF FREE STREAM FLOW FIELD DUE TO JET WAKE AND ANGLE OF ATTACK

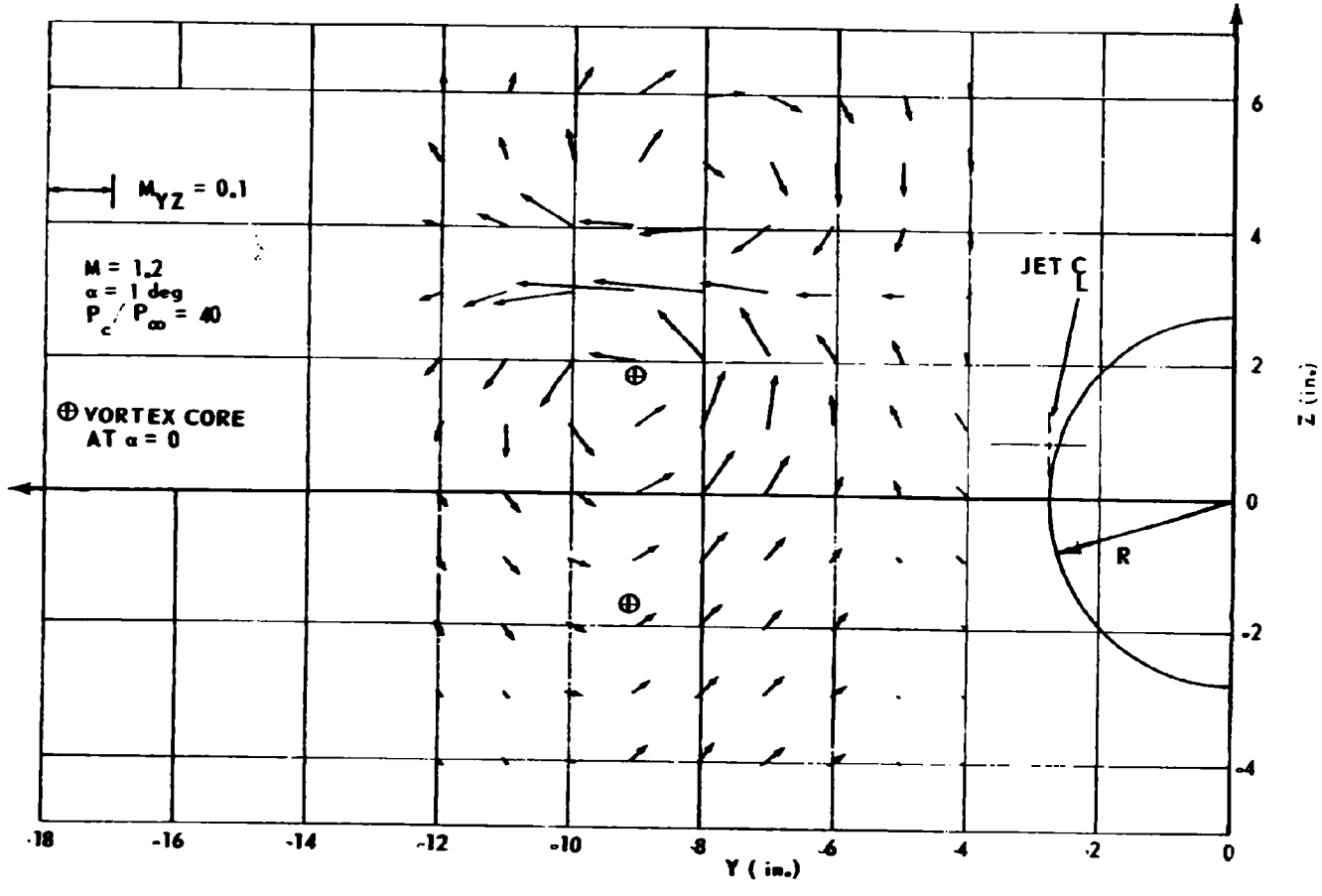

FIGURE 38. PERTURBATION OF FREE STREAM FLOW FIELD DUE TO JET WAKE AND ANGLE OF ATTACK

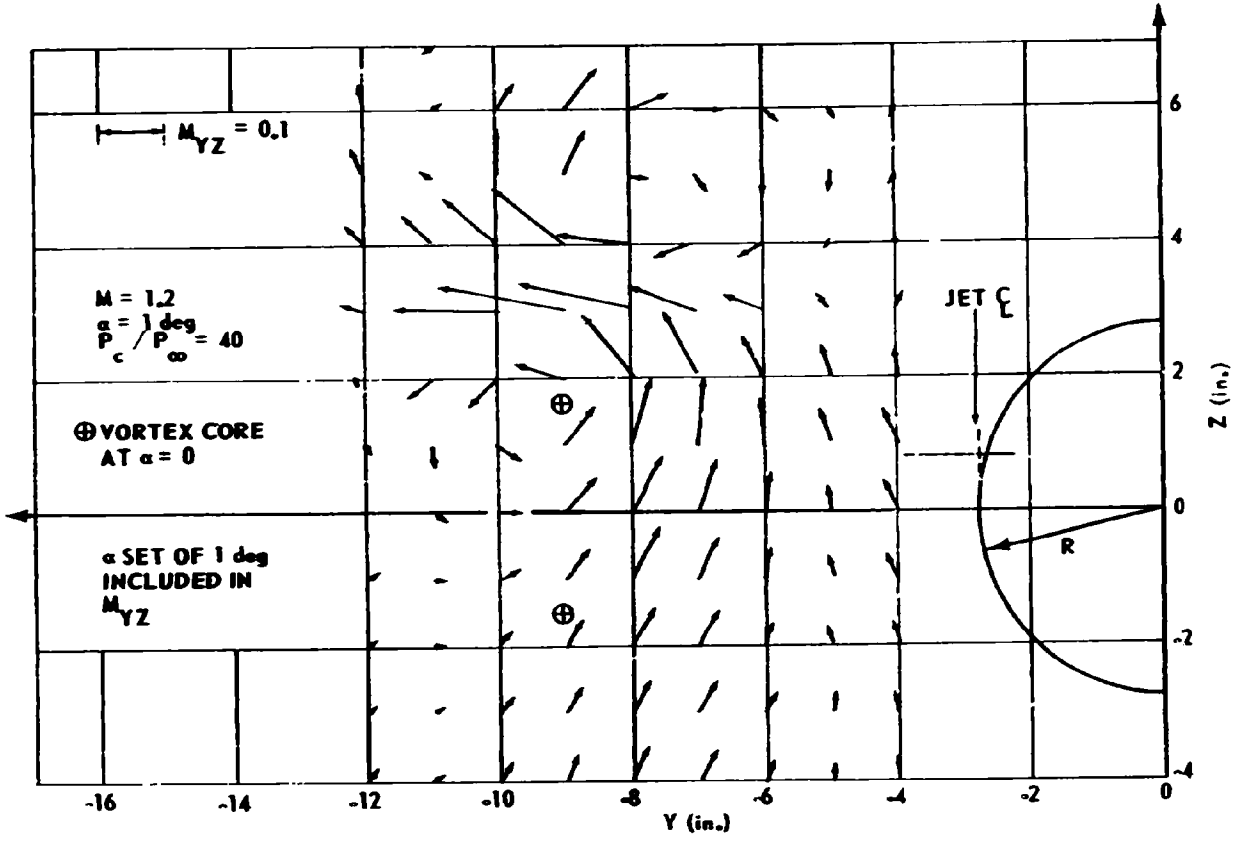

FIGURE 39. FREE STREAM FLOW FIELD DUE TO JET WAKE AND ANGLE OF ATTACK

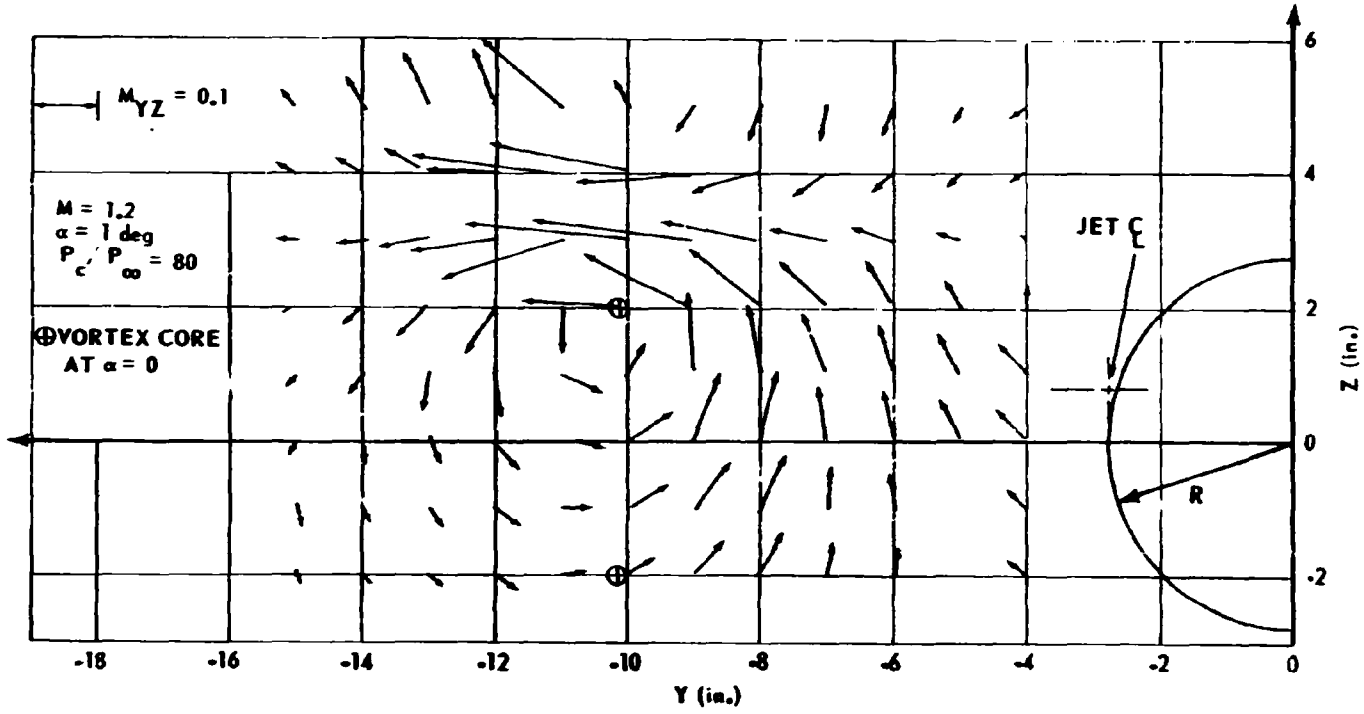

FIGURE 40. PERTURBATION OF FREE STREAM FLOW FIELD DUE TO JET WAKE AND ANGLE OF ATTACK

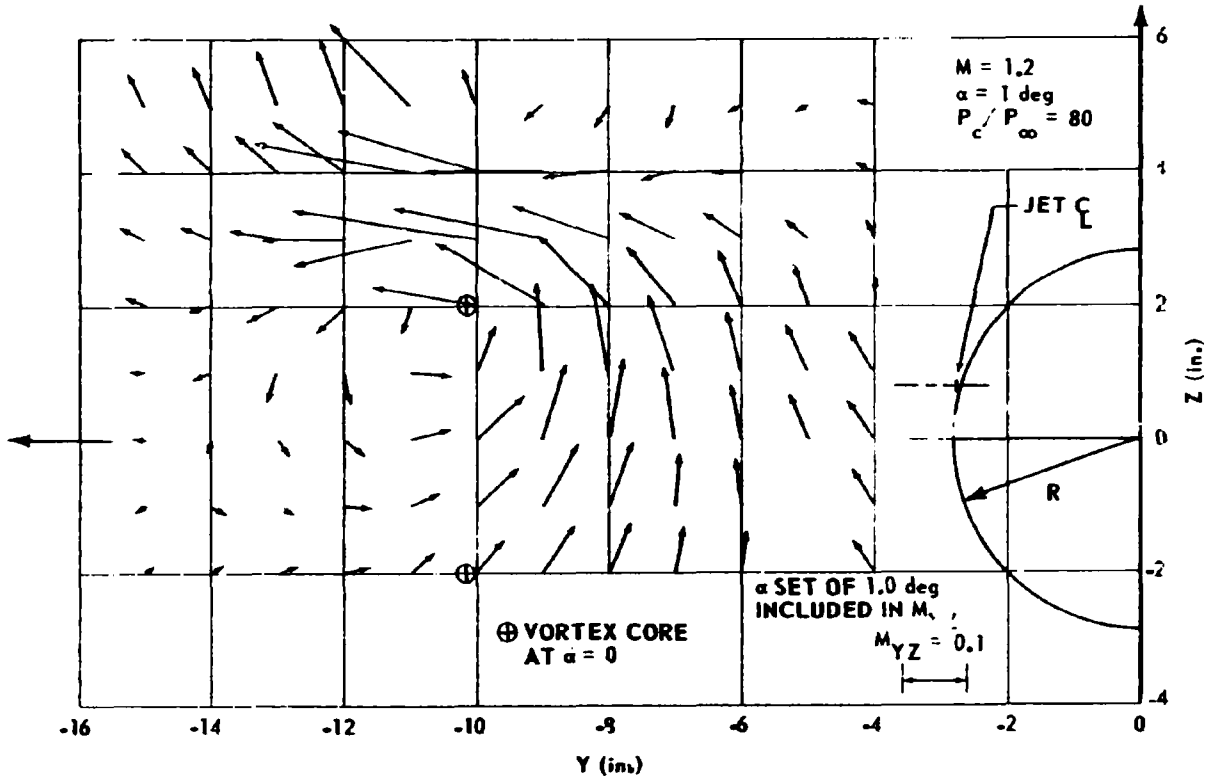

FIGURE 41. FREE STREAM FLOW FIELD DUE TO JET WAKE AND ANGLE OF ATTACK

REFERENCES

1. Chudyk, C. F., Flow Field Survey of a Typical Missile Configuration with a Forward-Mounted Control Jet Nozzle, Cornell Aeronautical Laboratory, Inc., Buffalo, New York, January 1968, Report No. AA-240-W-2.

2. Dahlke, C. W., An Experimental Investigation of Downstream Flow-Field Properties Behind a Forward Located Sonic Jet Injected into Transonic Freestream from a Body of Revolution, U. S. Army Missile Command, Redstone Arsenal, Alabama, January 1968, Report No. RD-TM-68-2.

3. Dahlke, C. W., Marks, A. S., and Deep, R. A., An Analysis of the Aerodynamic Interaction by Solid Propellant Gas Generator Exhaust for the LANCE Missile (U), U. S. Army Missile Command, Redstone Arsenal, Alabama, July 1966, Report No. RD-TM-66-10 (Confidential).

4. Burt, J. R., Jr., and Dahlke, C. W., Effects of Spin and Vent Tube Jet Flow on LANCE Missile Aerodynamic Coefficients from Analysis of Wind Tunnel Test, LTV Test 246 (U), U. S. Army Missile Command, Redstone Arsenal, Alabama, June 1967, Report No. RD-TM-67-4 (Confidential).

5. Dahlke, C. W., A Complete Summary of the Final Aerodynamic Coefficients for All Configurations Flown During the DC-MAW Exploratory Development Program (U), U. S. Army Missile Command, Redstone Arsenal, Alabama, May 1966, Report No. RD-TM-66-8 (Confidential).

6. Spring, D. J., and Martin, T. A., An Experimental Investigation at Transonic Speeds of the Effects of Forward Located Control Jets on the Aerodynamics of the Littlejohn Missile Employing the Thrust Floated Gyro System (U), U. S. Army Missile Command, Redstone Arsenal, Alabama, September 1966, Report No. RD-TM-66-13 (Confidential).

SELECTED BIBLIOGRAPHY

Pitts, W. C., Nielsen, J. N., and Kaattair, G. E., Lift and Center of Pressure of Wing-Body-Tail Combinations at Subsonic, Transonic, and Supersonic Speeds, 1959, NACA Report 1307.